

# Inhibitory signalling to the Arp2/3 complex steers cell migration

Irene Dang<sup>1\*</sup>, Roman Gorelik<sup>1\*</sup>, Carla Sousa-Blin<sup>1\*</sup>, Emmanuel Derivery<sup>1</sup>, Christophe Guérin<sup>2</sup>, Joern Linkner<sup>3</sup>, Maria Nemethova<sup>4</sup>, Julien G. Dumortier<sup>5</sup>, Florence A. Giger<sup>5</sup>, Tamara A. Chipysheva<sup>6</sup>, Valeria D. Ermilova<sup>6</sup>, Sophie Vacher<sup>7</sup>, Valérie Campanacci<sup>8</sup>, Isaline Herrada<sup>9</sup>, Anne-Gaelle Planson<sup>8</sup>, Susan Fetics<sup>8</sup>, Véronique Henriot<sup>1</sup>, Violaine David<sup>1</sup>, Ksenia Oguievetskaia<sup>1</sup>, Goran Lakisic<sup>1</sup>, Fabienne Pierre<sup>1</sup>, Anika Steffen<sup>10</sup>, Adeline Boyreau<sup>11</sup>, Nadine Peyriéras<sup>11</sup>, Klemens Rottner<sup>10,12</sup>, Sophie Zinn-Justin<sup>9</sup>, Jacqueline Cherfils<sup>8</sup>, Ivan Bièche<sup>7</sup>, Antonina Y. Alexandrova<sup>6</sup>, Nicolas B. David<sup>5</sup>, J. Victor Small<sup>4</sup>, Jan Faix<sup>3</sup>, Laurent Blanchoin<sup>2</sup> & Alexis Gautreau<sup>1</sup>

**Cell migration requires the generation of branched actin networks that power the protrusion of the plasma membrane in lamellipodia<sup>1,2</sup>. The actin-related proteins 2 and 3 (Arp2/3) complex is the molecular machine that nucleates these branched actin networks<sup>3</sup>. This machine is activated at the leading edge of migrating cells by Wiskott–Aldrich syndrome protein (WASP)-family verprolin-homologous protein (WAVE, also known as SCAR). The WAVE complex is itself directly activated by the small GTPase Rac, which induces lamellipodia<sup>4–6</sup>. However, how cells regulate the directionality of migration is poorly understood. Here we identify a new protein, Arpin, that inhibits the Arp2/3 complex *in vitro*, and show that Rac signalling recruits and activates Arpin at the lamellipodial tip, like WAVE. Consistently, after depletion of the inhibitory Arpin, lamellipodia protrude faster and cells migrate faster. A major role of this inhibitory circuit, however, is to control directional persistence of migration. Indeed, Arpin depletion in both mammalian cells and *Dictyostelium discoideum* amoeba resulted in straighter trajectories, whereas Arpin microinjection in fish keratocytes, one of the most persistent systems of cell migration, induced these cells to turn. The coexistence of the Rac–Arpin–Arp2/3 inhibitory circuit with the Rac–WAVE–Arp2/3 activatory circuit can account for this conserved role of Arpin in steering cell migration.**

The Arp2/3 complex is activated at different cellular locations by different nucleation promoting factors (NPFs), WAVE at lamellipodia, neural WASP (N-WASP) at clathrin-coated pits, and WASP and SCAR homologue (WASH) at endosomes<sup>7,8</sup>. NPFs share a characteristic carboxy-terminal tripartite domain, referred to as the VCA<sup>9</sup>. The A (acidic) motif binds to the Arp2/3 complex and induces its conformational activation. Arp2/3 inhibitory proteins containing an A motif, PICK1 and Gadkin (also known as AP1AR and  $\gamma$ -BAR), were detected at endocytic pits and at endosomes<sup>10,11</sup>. Thus, although endocytic pits and endosomes possess antagonistic activities towards the Arp2/3 complex, it was not known whether lamellipodia contain a similar Arp2/3 inhibitory protein to counteract WAVE. To identify such a protein, we performed a bioinformatics search for proteins displaying the typical A motif of human NPFs, characterized by a tryptophan residue at the antepenultimate position in an acidic context. We identified an uncharacterized protein (C15orf38) clustered with NPFs with this procedure (Fig. 1a). This protein was named Arpin. Arpin is encoded by a single gene in metazoans and amoeba. Predictions and NMR analysis indicate that this protein of about 220 residues is structured

with the exception of its highly mobile C-terminal end, which contains the putative Arp2/3-binding site (Extended Data Figs 1 and 2). Indeed, Arpin binds to Arp2/3 mostly through its acidic motif (Fig. 1b and Extended Data Figs 3 and 4).

The molecular function of Arpin on Arp2/3 activity was assayed by spectrofluorimetry and total internal reflection fluorescence (TIRF) microscopy using purified proteins. Arpin was unable to activate the Arp2/3 complex, consistent with its lack of verprolin (V) and cofilin (C) homology motifs. However, when Arp2/3 was activated by VCA, Arpin, but not its truncated form lacking the acidic motif (Arpin $\Delta$ A), inhibited actin polymerization in a dose-dependent manner (Fig. 1c). The acidic peptide was sufficient for this inhibition, although it was less effective than full-length Arpin, in line with its lower affinity for the Arp2/3 complex (Extended Data Fig. 4). Arpin inhibited Arp2/3 activation, because we observed by TIRF microscopy the generation of fewer actin branched junctions in the presence of Arpin (Fig. 1d and Supplementary Video 1). Full-length Arpin and its acidic motif, but not Arpin $\Delta$ A, compete with VCA for Arp2/3 binding (Fig. 1e and Extended Data Fig. 4). Therefore, Arpin is a new competitive inhibitor of the Arp2/3 complex. The name Arpin is a mnemonic for its activity (Arp2/3 inhibition).

The subcellular localization of Arpin was examined by immunofluorescence in spreading mouse embryonic fibroblasts (MEFs). Arpin was detected in restricted segments of the plasma membrane, which were also stained by three lamellipodial markers—the WAVE complex, the Arp2/3 complex and cortactin (Fig. 2a and Extended Data Fig. 5). Radial line scans of immunofluorescence pictures through lamellipodial outlines were generated, registered with the edge as a reference, and averaged to reveal the relative distributions of these different lamellipodial components. Arpin overlapped perfectly with the distribution of the WAVE complex, a tip component<sup>12</sup> (Fig. 2a). Arpin is thus localized at the lamellipodium tip, where new actin branches are nucleated by WAVE and Arp2/3 complexes. As expected, Arp2/3 and cortactin distribution extended rearwards compared to Arpin (Extended Data Fig. 5), because Arp2/3 and cortactin correspond to branches of the lamellipodial actin network undergoing retrograde flow with respect to the protruding membrane<sup>9,13</sup>.

To understand the regulation of Arpin activity, we examined the role of Rac, the master controller of lamellipodium formation. We co-transfected 293T cells with different forms of Rac and green fluorescent protein (GFP)–Arpin and then analysed the interaction of

<sup>1</sup>Group Cytoskeleton in Cell Morphogenesis, Laboratoire d'Enzymologie et Biochimie Structurales, CNRS UPR3082, Gif-sur-Yvette 91190, France. <sup>2</sup>Institut de Recherches en Technologies et Sciences pour le Vivant (iRTSV), Laboratoire de Physiologie Cellulaire et Végétale, CNRS/CEA/INRA/UJF, Grenoble 38054, France. <sup>3</sup>Institute for Biophysical Chemistry, Hannover Medical School, Hannover 30625, Germany. <sup>4</sup>Institute of Molecular Biotechnology, Vienna 1030, Austria. <sup>5</sup>INSERM U1024, CNRS UMR8197, ENS, Institut de Biologie de l'ENS, Paris 75005, France. <sup>6</sup>Institute of Carcinogenesis, N. N. Blokhin Cancer Research Center, Russian Academy of Medical Sciences, Moscow 115478, Russia. <sup>7</sup>Oncogenetic Laboratory, Institut Curie, Hôpital René Huguenin, Saint-Cloud 92210, France. <sup>8</sup>Group Small G Proteins, Laboratoire d'Enzymologie et Biochimie Structurales, CNRS UPR3082, Gif-sur-Yvette 91190, France. <sup>9</sup>Laboratoire de Biologie Structurale et Radiobiologie (iBiTec-S), CNRS URA2096, CEA Saclay, Gif-sur-Yvette 91190, France. <sup>10</sup>Institute of Genetics, University of Bonn, Bonn 53115, Germany. <sup>11</sup>Institut des Systèmes Complexes & NeD, Institut de Neurobiologie Alfred Fessard, CNRS UPR3294, Gif-sur-Yvette 91190, France. <sup>12</sup>Helmholtz Centre for Infection Research, Braunschweig 38124, Germany.

\*These authors contributed equally to this work.

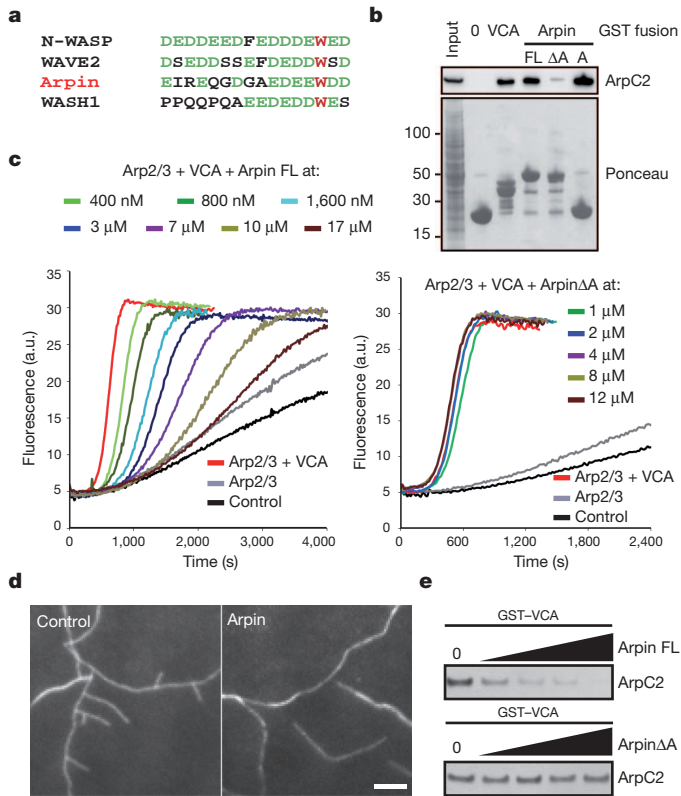


**Figure 1 | Arpin inhibits Arp2/3 activation *in vitro*.** **a**, Alignment of acidic C termini of three NPFs and of Arpin. **b**, Arpin binds to the Arp2/3 complex through its acidic C-terminal region. Glutathione S-transferase (GST) pull-down with full-length Arpin (FL), its last 16 amino-acids (A), ArpinΔA or the VCA domain of N-WASP as a positive control. ArpC2 is a subunit of the Arp2/3 complex. **c**, Spectrofluorimetry assay using pyrene-labelled actin to monitor polymerization. a.u., arbitrary units. **d**, Assembly of branched actin networks monitored by TIRF microscopy using rhodamine-labelled actin. Scale bar, 5 μm. **e**, Full-length Arpin, but not ArpinΔA (18 μM and serial twofold dilutions), competes with the NPF for Arp2/3 binding.

Arpin with the Arp2/3 complex through GFP immunoprecipitations. The active form of Rac1, which is sufficient to induce lamellipodia, was also sufficient to induce Arp2/3 co-immunoprecipitation with Arpin (Fig. 2b). To examine whether Rac is required for Arpin activation, we used Rac1 knockout MEFs that lack lamellipodia<sup>14</sup>. The absence of Rac abrogated the peripheral localization of Arpin in all knockout MEF cells examined (Extended Data Fig. 5). Endogenous Arpin was then immunoprecipitated from Rac1 knockout MEFs. The Arp2/3 complex co-immunoprecipitated with Arpin in control MEF cells, but not in Rac-deficient cells (Fig. 2c). Together, these results show that, in response to Rac signalling, Arpin inhibits the Arp2/3 complex at the lamellipodium tip, that is, where Rac also stimulates actin polymerization through the WAVE complex.

This counterintuitive finding suggests that Arpin would be a built-in brake of protrusions. Human RPE1 cells transiently transfected with short hairpin RNAs (shRNA) that efficiently deplete Arpin displayed increased lamellipodia-mediated cell spreading (Extended Data Fig. 6 and Supplementary Video 2). Arpin depletion increased protrusion velocity of lamellipodia, consistent with its Arp2/3 inhibitory role (Fig. 2d). This effect was fully rescued by Arpin re-expression, but only when Arpin contained the acidic motif. Arpin thus provides a paradoxical negative circuit downstream of Rac. Such a circuitry, where Rac induces and inhibits actin polymerization, generates an 'incoherent feedforward loop' (Fig. 2e), which can favour temporal regulations<sup>15</sup>.

To examine whether the Arpin circuit is physiologically relevant for cell migration, we impaired the expression of the *arpin* gene in zebrafish embryos using morpholinos. During gastrulation, prechordal plate

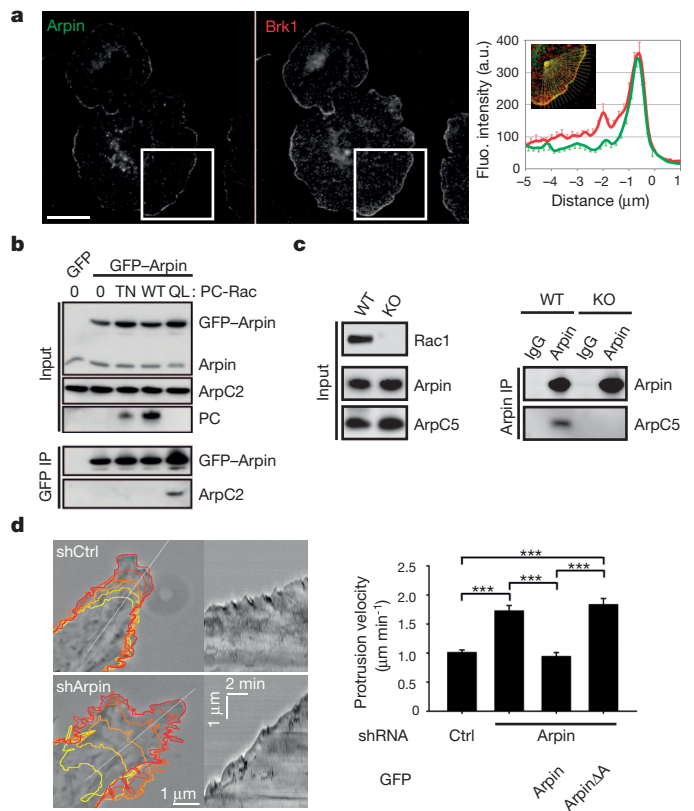


**Figure 2 | Arpin inhibits the Arp2/3 complex at the lamellipodium tip.** **a**, Arpin colocalizes with Brk1, a subunit of the WAVE complex, at the lamellipodium tip (mean ± s.e.m., 24 line scans). Scale bar, 20 μm. **b**, Active (Gln61Leu; QL), but not wild-type (WT), nor dominant negative (Thr17Asn; TN), Rac induces Arpin association with the Arp2/3 complex. IP, immunoprecipitation. PC, protein C epitope. **c**, Rac is required for the Arpin-Arp2/3 interaction. KO, knockout. **d**, Arpin depletion increases the speed at which lamellipodia protrude. GFP-Arpin expression rescues the phenotype. Ctrl, control; shCtrl, control shRNA; shArpin, *arpin* shRNA. Data are mean ± s.e.m.;  $n = 40$ ;  $***P < 0.001$ , two-tailed analysis of variance (ANOVA). **e**, Arpin circuitry.

cells collectively migrate towards the animal pole. After *arpin* loss of function, cell movements were less coordinated (Extended Data Fig. 7). Prechordal plate cell transplants revealed a cell autonomous effect of Arpin on protrusions. Protrusions were more frequent and more persistent over time in the absence of Arpin (Supplementary Video 3). This observation is consistent with the incoherent feedforward loop, a circuitry that can suppress the protrusion it creates.

To understand the role of the incoherent feedforward loop in cell migration further, we performed Arpin loss-of-function experiments in cell systems migrating as individual cells. Migration of stable Arpin-depleted clones from the breast human cell line MDA-MB-231 was analysed by video microscopy in two or three dimensions (Fig. 3a, Supplementary Videos 4 and 5, and Extended Data Fig. 8). In both cases, the tracks illustrate that Arpin-depleted cells explored a larger territory than control cells, an observation substantiated by mean square displacements (Extended Data Fig. 9). Increased exploration was not only due to increased speed, but also to increased directional persistence, measured as the ratio of the distance between two points by the actual trajectory (Fig. 3a) or as the direction autocorrelation function (Extended Data Fig. 10). Because Arpin is conserved in amoeba,

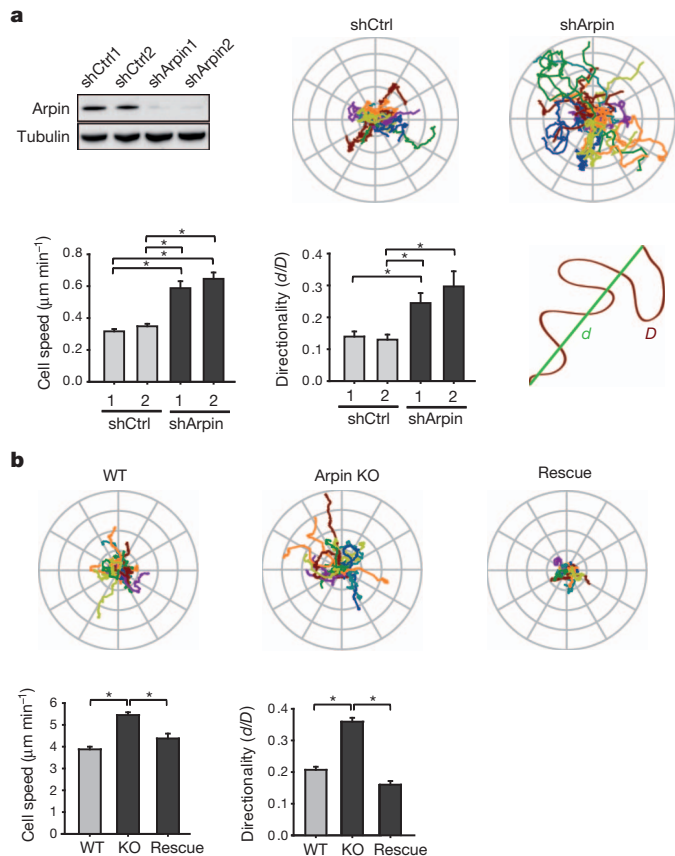


**Figure 3 | Arpin depletion increases directional persistence of migration in mammalian cells and in *Dictyostelium discoideum*.** **a**, Arpin-depleted (shArpin1 and shArpin2) MDA-MB-231 cells explore a wider territory than controls owing to increased speed and directional persistence. The directionality index is calculated as the ratio of the distance between starting and ending points ( $d$ ) by the actual trajectory ( $D$ ). Mean  $\pm$  s.e.m.;  $n = 24, 31, 32$  and  $26$ , respectively;  $*P < 0.05$ , two-tailed Kruskal–Wallis test. **b**, Arpin-knockout amoeba explores a wider territory than wild type owing to increased speed and directional persistence. Directionality is more than fully rescued by *Dictyostelium* Arpin expression in knockout amoeba. Data are mean  $\pm$  s.e.m.;  $n = 116, 196$  and  $45$ , respectively;  $*P < 0.05$ , two-tailed Kruskal–Wallis test.

we analysed its function in *Dictyostelium discoideum* by knocking out the orthologous gene. As in mammalian cells, Arpin-knockout *Dictyostelium* amoebae explored a wider territory than the controls owing to increased cell speed and directional persistence (Fig. 3b and Supplementary Video 6). However, directional persistence, which is more than fully rescued by GFP–Arpin expression, is the most affected parameter in amoeba.

Arpin could thus be a ‘steering factor’. To test this hypothesis directly in a gain-of-function experiment, we selected the fish keratocyte model. These cells are characterized by fast migration based on a wide fan-shaped lamellipodium with high directional persistence. We purified zebrafish Arpin and Arpin $\Delta A$  from *Escherichia coli* and microinjected these proteins into migrating trout keratocytes (Fig. 4a). Injection of Arpin, but not Arpin $\Delta A$ , caused keratocytes to reduce their speed and deviate from their initial direction of migration (Fig. 4b and Extended Data Fig. 10). Notably, Arpin did not prevent lamellipodia protrusion, but resulted in cycles of suppression of existing lamellipodia followed by formation of new, ectopic ones (Fig. 4c and Supplementary Video 7). Collectively, the experiments performed in different systems of cell migration support a role for Arpin in promoting cell steering: Arpin slows cells down and allows them to turn.

In a computational model of efficient and persistent cell migration, the lamellipodium spatially determines where the WAVE and the Arp2/3 complexes will next polymerize actin, thus maintaining the

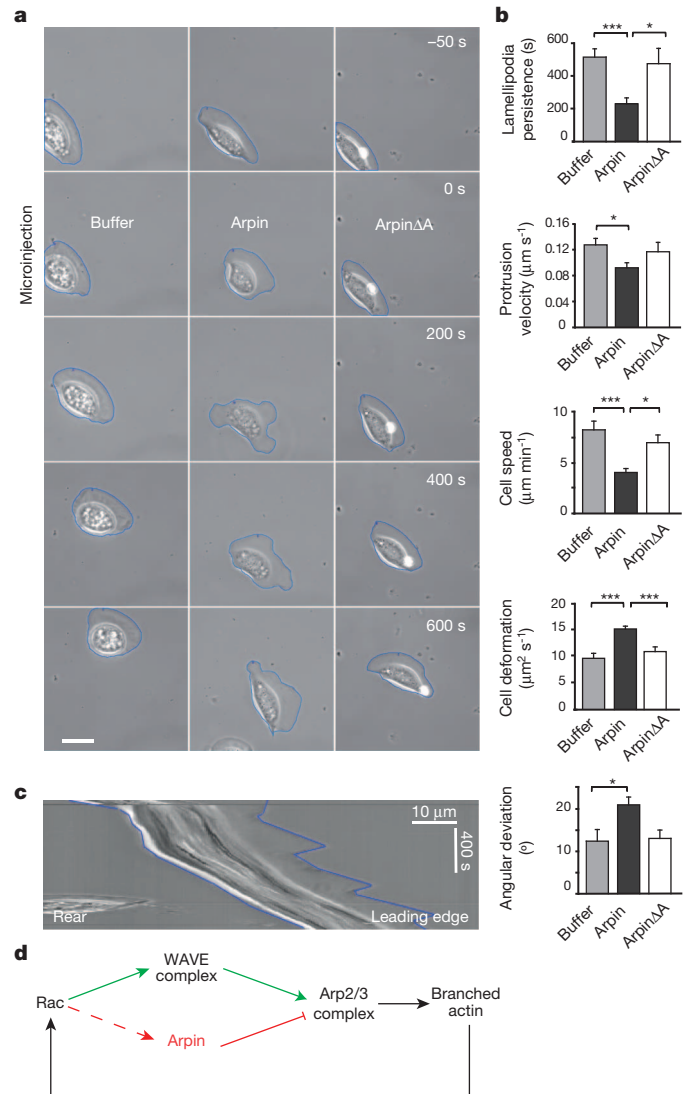


**Figure 4 | Arpin microinjection induces fish keratocyte to turn.** **a**, Gallery of fish keratocytes microinjected with purified full-length Arpin, Arpin $\Delta A$  or buffer as control. Scale bar,  $20 \mu\text{m}$ . **b**, Quantifications. Data are mean  $\pm$  s.e.m.;  $n = 16, 15$  and  $11$ , respectively;  $*P < 0.05$ ,  $***P < 0.001$ , two-tailed ANOVA. **c**, Kymograph of the Arpin-microinjected keratocyte. **d**, Model.

front at the front over time<sup>16</sup> (Fig. 4d). Such a feedback loop, sensing where branched actin is polymerized and activating Rac as a response, has recently been identified: it involves coronin 1A and the Rac exchange factor  $\beta$ -Pix<sup>17</sup>. In this feedback system, the WAVE complex closes a positive feedback loop that maintains efficient directional migration over time, whereas Arpin closes a concurrent negative feedback loop, which induces braking and allows turning. These two nested feedback loops, positive and negative, can account for the emergence of oscillations in lamellipodium protrusion/retraction, as observed in fish keratocytes after Arpin injection (Supplementary Video 8), and for various travelling actin waves described in different systems<sup>18–21</sup>.

Other proteins were previously shown to regulate cell steering<sup>22,23</sup>. Knockdown of Rac1 or cofilin, a protein that severs and depolymerizes actin filaments, increases directional persistence of mammalian cells<sup>24,25</sup>. These proteins are required, however, for lamellipodial protrusion and actin-based motility<sup>26,27</sup>. Arpin is unique in that it regulates cell steering, while being dispensable for lamellipodial protrusion and efficient migration. Arpin is a prime candidate to fine-tune numerous physiological migrations biased by diverse cues<sup>23</sup>. Arpin also seems to have a role in preventing cells from migrating. In this respect, dissection of the

mechanisms regulating Arpin in physiology and pathology is a major challenge ahead of us.

## METHODS SUMMARY

**Arpin purification and antibody production.** Arpin was purified from *E. coli* as a glutathione S-transferase (GST) fusion protein and cleaved off GST. Untagged Arpin was used for *in vitro* assays of actin polymerization, antibody generation and keratocyte injection. Rabbit polyclonal antibodies targeting full-length Arpin were purified by affinity chromatography. Immunoprecipitation of endogenous Arpin was performed using purified antibodies coupled to magnetic beads.

**Cells and imaging.** RPE1 cells were electroporated with plasmids. Plasmids encoding fusion proteins or shRNAs were transfected into MDA-MB-231 cells using liposomes. Lamellipodial dynamics and random migration were analysed with ImageJ using the plug-ins 'Kymograph' and 'MtrackJ', respectively. Live-cell imaging was performed using an inverted Axio Observer microscope (Zeiss) equipped with two chambers controlled for temperature and CO<sub>2</sub>. For Arpin localization, MEF cells were fixed with 10% TCA, permeabilized with 0.2% Triton X-100, and processed for immunofluorescence. To draw radial line scans, a custom-made ImageJ plug-in was developed, edge was determined using 'Isodata' and 'Analyze particle', and then a custom-made VBA macro in Excel was used to align data relative to the edge. Keratocytes were isolated from scales of freshly killed brook trout (*Salvelinus fontinalis*) and microinjected with a Femtojet (Eppendorf). Plots were drawn with SigmaPlot (SPSS) and statistics were performed with SigmaStat (SPSS).

**Online Content** Any additional Methods, Extended Data display items and Source Data are available in the online version of the paper; references unique to these sections appear only in the online paper.

Received 21 November 2012; accepted 28 August 2013.

Published online 16 October 2013.

- Wu, C. *et al.* Arp2/3 is critical for lamellipodia and response to extracellular matrix cues but is dispensable for chemotaxis. *Cell* **148**, 973–987 (2012).
- Suraneni, P. *et al.* The Arp2/3 complex is required for lamellipodia extension and directional fibroblast cell migration. *J. Cell Biol.* **197**, 239–251 (2012).
- Mullins, R. D., Heuser, J. A. & Pollard, T. D. The interaction of Arp2/3 complex with actin: nucleation, high affinity pointed end capping, and formation of branching networks of filaments. *Proc. Natl Acad. Sci. USA* **95**, 6181–6186 (1998).
- Insall, R. H. & Machesky, L. M. Actin dynamics at the leading edge: from simple machinery to complex networks. *Dev. Cell* **17**, 310–322 (2009).
- Padrick, S. B. & Rosen, M. K. Physical mechanisms of signal integration by WASP family proteins. *Annu. Rev. Biochem.* **79**, 707–735 (2010).
- Ridley, A. J. Life at the leading edge. *Cell* **145**, 1012–1022 (2011).
- Derivery, E. *et al.* The Arp2/3 activator WASH controls the fission of endosomes through a large multiprotein complex. *Dev. Cell* **17**, 712–723 (2009).
- Suetsugu, S. & Gautreau, A. Synergistic BAR-NPF interactions in actin-driven membrane remodeling. *Trends Cell Biol.* **22**, 141–150 (2012).
- Pollard, T. D. Regulation of actin filament assembly by Arp2/3 complex and formins. *Annu. Rev. Biophys. Biomol. Struct.* **36**, 451–477 (2007).
- Rocca, D. L., Martin, S., Jenkins, E. L. & Hanley, J. G. Inhibition of Arp2/3-mediated actin polymerization by PICK1 regulates neuronal morphology and AMPA receptor endocytosis. *Nature Cell Biol.* **10**, 259–271 (2008).
- Maritzen, T. *et al.* Gadin negatively regulates cell spreading and motility via sequestration of the actin-nucleating ARP2/3 complex. *Proc. Natl Acad. Sci. USA* **109**, 10382–10387 (2012).
- Lai, F. P. *et al.* Arp2/3 complex interactions and actin network turnover in lamellipodia. *EMBO J.* **27**, 982–992 (2008).
- Cai, L., Makhov, A. M., Schafer, D. A. & Bear, J. E. Coronin 1B antagonizes cortactin and remodels Arp2/3-containing actin branches in lamellipodia. *Cell* **134**, 828–842 (2008).
- Steffen, A. *et al.* Rac function is critical for cell migration but not required for spreading and focal adhesion formation. *J. Cell Sci.* <http://dx.doi.org/10.1242/jcs.118232> (31 July 2013).
- Hart, Y. & Alon, U. The utility of paradoxical components in biological circuits. *Mol. Cell* **49**, 213–221 (2013).
- Neilson, M. P. *et al.* Chemotaxis: a feedback-based computational model robustly predicts multiple aspects of real cell behaviour. *PLoS Biol.* **9**, e1000618 (2011).
- Castro-Castro, A. *et al.* Coronin 1A promotes a cytoskeletal-based feedback loop that facilitates Rac1 translocation and activation. *EMBO J.* **30**, 3913–3927 (2011).
- Machacek, M. & Danuser, G. Morphodynamic profiling of protrusion phenotypes. *Biophys. J.* **90**, 1439–1452 (2006).
- Weiner, O. D., Marganski, W. A., Wu, L. F., Altschuler, S. J. & Kirschner, M. W. An actin-based wave generator organizes cell motility. *PLoS Biol.* **5**, e221 (2007).
- Brandman, O. & Meyer, T. Feedback loops shape cellular signals in space and time. *Science* **322**, 390–395 (2008).
- Allard, J. & Mogilner, A. Traveling waves in actin dynamics and cell motility. *Curr. Opin. Cell Biol.* **25**, 107–115 (2013).
- Ghosh, M. *et al.* Cofilin promotes actin polymerization and defines the direction of cell motility. *Science* **304**, 743–746 (2004).
- Petrie, R. J., Doyle, A. D. & Yamada, K. M. Random versus directionally persistent cell migration. *Nature Rev. Mol. Cell Biol.* **10**, 538–549 (2009).
- Pankov, R. *et al.* A Rac switch regulates random versus directionally persistent cell migration. *J. Cell Biol.* **170**, 793–802 (2005).
- Sidani, M. *et al.* Cofilin determines the migration behavior and turning frequency of metastatic cancer cells. *J. Cell Biol.* **179**, 777–791 (2007).
- Li, A. *et al.* Rac1 drives melanoblast organization during mouse development by orchestrating pseudopod-driven motility and cell-cycle progression. *Dev. Cell* **21**, 722–734 (2011).
- Loisel, T. P., Boujema, R., Pantaloni, D. & Carlier, M. F. Reconstitution of actin-based motility of *Listeria* and *Shigella* using pure proteins. *Nature* **401**, 613–616 (1999).

**Supplementary Information** is available in the online version of the paper.

**Acknowledgements** A.G. acknowledges his PhD supervisor M. Arpin, the name of the here identified protein is a tribute to her mentoring. We thank G. Romet-Lemonne, E. Portnoy and F. Marletaz for suggestions. We acknowledge support from Agence Nationale pour la Recherche (ANR-08-BLAN-0012-CSD 8 to A.G. and L.B., ANR-08-PCVI-0010-03 to A.G., ANR-11-BSV8-0010-02 to A.G., J.C. and S.Z.-J.), Association pour la Recherche sur le Cancer (SFI20101201512 to A.G., PDF20111204331 to R.G., SFI20111203770 to N.B.D.), the Bio-Emergences IBISA facility and Fundacao para a Ciencia e a Tecnologia (SFRH/BPD/46451/2008 to C.S.-B.), the Austrian Science Fund (FWF P21292-B09 to J.V.S.), the Deutsche Forschungsgemeinschaft (FA 330/5-1 to J.F.) and grant number 8066, code 2012-1.1-12-000-1002-064 from the Russian Ministry of Education and Science to A.Y.A.

**Author Contributions** I.D., R.G. and C.S.-B. performed videomicroscopy, analysed cell migration, analysed biochemical interactions of Arpin and its localization. E.D. wrote the bioinformatics programme that first identified Arpin. C.G. and L.B. performed *in vitro* actin polymerization and fluorescence anisotropy assays. J.L. and J.F. isolated knockout amoeba and analysed their migration. M.N. and J.V.S. micro-injected fish keratocytes. J.G.D., F.A.G. and N.B.D. characterized the Arpin phenotype in zebrafish. A.B. and N.P. determined the Arpin expression profile in zebrafish. I.H. and S.Z.-J. contributed the NMR spectrum. T.A.C., V.D.E., A.Y.A., S.V., I.B., V.C., V.D., G.L., K.O., F.P., A.-G.P., S.F. and V.H. generated DNA constructs, isolated stable cell clones, purified and characterized recombinant proteins, and performed crucial experiments for our understanding of Arpin function. A.S. and K.R. isolated the Rac1 knockout MEFs. All authors designed experiments. N.P., K.R., S.Z.-J., J.C., N.B.D., I.B., A.Y.A., J.V.S., J.F., L.B. and A.G. supervised the work in their respective research group. A.G. coordinated the study and wrote the paper.

**Author Information** Reprints and permissions information is available at [www.nature.com/reprints](http://www.nature.com/reprints). The authors declare no competing financial interests. Readers are welcome to comment on the online version of the paper. Correspondence and requests for materials should be addressed to A.G. ([alexis.gautreau@lebs.cnrs-gif.fr](mailto:alexis.gautreau@lebs.cnrs-gif.fr))

## METHODS

**Plasmids.** Human and zebrafish Arpin were amplified by PCR from clones IMAGE:5770387 and IMAGE:7404342, respectively (GeneService). *Dictyostelium discoideum* DdArpin was amplified from Ax2 cDNA. Human full-length Arpin (residues 1–226), Arpin $\Delta$ A (residues 1–210) or ArpinA (residues 211–226), zebrafish full-length Arpin (residues 1–226), Arpin $\Delta$ A (residues 1–210), and murine N-WASP VCA fragment (residues 392–501)<sup>28</sup> were cloned into a modified pGEX vector with a TEV cleavage site between the restriction sites FseI and AscI. For expression in mammalian cells, Arpin inserts were cloned into a compatible plasmid pcDNAm PC-GFP blue<sup>7</sup>. Zebrafish full-length Arpin was also inserted pBluescript to generate probes for *in situ* hybridization and in pCS2-GFP for rescue experiments. Human RAC1 wild-type, Thr17Asn, Gln61Leu, the Arp2/3 complex subunits ArpC5A and ArpC5B<sup>29</sup> were cloned into pcDNA5 His PC TEV blue<sup>7</sup>. For expression in amoeba, *Dictyostelium* Arpin was inserted into pDGFP-MCS-neo<sup>30</sup>. For shRNA-expressing plasmids, two hybridized oligonucleotides (MWG) were cloned into psiRNA-h7SKblasti G1 (Invivogen) according to the manufacturer's protocol. The following target sequences were used: shArpin 1: 5'-GGAGAAGCTGATCGATGTATCT-3'; shArpin 2: 5'-GCTTCCTCATGT CGTCTACA-3'; shArpin 3: 5'-GCCTTCCTAGACATTACATGA-3' (targets the 3' untranslated region (UTR) of *arpin* mRNA); shArpC2 1: 5'-CATGTATGT TGAGTCTAA-3'; and shArpC2 2: 5'-GCTCTAAGGCCTATATTC-3'. These plasmids were compared to the non-targeting control provided by Invivogen; shControl: 5'-GCATATGTGCGTACCTAGCAT-3'. All constructs were verified by sequencing.

**Protein purification.** Arpin, Arpin $\Delta$ A, ArpinA and N-WASP VCA fused to GST were purified from *E. coli* BL21\* strain (Life Technologies) using standard purification protocols, dialysed against storage buffer (20 mM Tris-HCl, 50 mM NaCl, 1 mM dithiothreitol (DTT), pH 7.5), frozen in liquid nitrogen and stored at  $-80^{\circ}\text{C}$ . When indicated, Arpin was cleaved by TEV protease off GST. Arpin bound to glutathione sepharose 4B beads was cleaved by overnight incubation at  $4^{\circ}\text{C}$  using His-tagged TEV protease in 50 mM Tris, pH 7.5, 2 mM  $\beta$ -mercaptoethanol, 100 mM NaCl and 5 mM MgCl<sub>2</sub>. TEV was removed by incubation with Ni<sup>2+</sup> beads (GE Healthcare). Arpin was further purified by size-exclusion chromatography (SEC) on a Superdex-200 column (GE Healthcare) and concentrated on Vivaspin filters. Human Arpin was used for the production of polyclonal antibodies and competition experiments. Zebrafish Arpin was similarly produced, purified and used for keratocyte injection at  $7.5\ \mu\text{g}\ \mu\text{l}^{-1}$  in 15 mM Tris-HCl, 150 mM NaCl, 5 mM MgCl<sub>2</sub> and 1 mM DTT, pH 7.5. Both proteins had an amino-terminal extension of 10 amino acids (GAMAHMGRP) after TEV cleavage. ArpinA peptide (residues 211–226 of full-length Arpin) was purchased from Proteogenix. For the SEC coupled to multiangle light scattering (SEC-MALS) characterization, proteins were separated in a 15-ml KW-803 column (Shodex) run on a Shimadzu HPLC system. MALS, quasi-elastic light scattering (QELS) and refractive index (RI) measurements were achieved with a MiniDawn Treos (Wyatt technology), a WyattQELS (Wyatt technology) and an Optilab T-rEX (Wyatt technology), respectively. Molecular mass and hydrodynamic radius calculations were performed with the ASTRA VI software (Wyatt Technology) using a  $dn/dc$  value of  $0.183\ \text{ml}\ \text{g}^{-1}$ .

**Antibodies.** Polyclonal antibodies targeting Arpin were obtained in rabbits (AgroBio) against purified human Arpin, and then purified by affinity purification on a HiTrap NHS-activated HP column (GE Healthcare) coupled to the immunogen. ArpC2 polyclonal antibody and cortactin monoclonal antibody (clone 4F11) were from Millipore. ArpC5 monoclonal antibody (clone 323H3) was from Synaptic Systems. Brk1 monoclonal antibody (clone 231H9) was described earlier<sup>31</sup>. Tubulin monoclonal antibody (clone E7) was obtained from Developmental Studies Hybridoma Bank. PC monoclonal antibody (clone HPC4) was from Roche.

**In vitro assays of actin polymerization.** Pyrene actin assays and monitoring of the branching reaction were performed as described previously<sup>32</sup>. VCA refers to the VCA domain of WAVE1 purified as described<sup>33</sup>. Conditions for Fig. 1c were: 2  $\mu\text{M}$  actin (10% pyrene-labelled), 500 nM VCA, 20 nM Arp2/3 and Arpin full-length or Arpin $\Delta$ A at the indicated concentrations. Conditions for Fig. 1d were: 1  $\mu\text{M}$  actin (10% rhodamine-labelled), 150 nM VCA, 80 nM Arp2/3 and 5  $\mu\text{M}$  Arpin when indicated.

**Fluorescence anisotropy based determination of  $K_d$ .** The ArpinA peptide was synthesized and labelled with 5-TAMRA at the amino terminus (Proteogenix). The peptide was excited with polarized light at 549 nm and emitted light was detected at 573 nm using a MOS450 fluorimeter (Biologic). Measurements were made for 60 s at 1 point  $\text{s}^{-1}$ , and the average anisotropy was calculated with the Biologic software. Fits were performed as described previously<sup>34</sup>.

**GST pull-down, immunoprecipitations, SDS-PAGE and western blots.** HeLa cells were lysed in 50 mM Tris-HCl, 150 mM NaCl, 1 mM EDTA, 1 mM DTT, 0.5% Triton X-100 and 5% glycerol, pH 7.5. GST fusion protein (20  $\mu\text{g}$ ) associated with 20  $\mu\text{l}$  of glutathione sepharose 4B beads (GE Healthcare) was incubated with

1 ml HeLa cell extracts for 2 h at  $4^{\circ}\text{C}$ . Beads were washed and analysed by western blot.

Co-immunoprecipitation of Arpin with the Arp2/3 complex was performed with either two 15-cm dishes of MEF cells, or one 10-cm dish of transfected 293T cells. Cell lysates prepared in 10 mM HEPES, pH 7.7, 50 mM KCl, 1 mM MgCl<sub>2</sub>, 1 mM EGTA and 1% Triton X-100 were incubated with 10  $\mu\text{g}$  of non-immune rabbit IgG or 10  $\mu\text{g}$  of anti-Arpin antibodies coupled to tosyl-activated dynabeads (Life Technologies) or to GFP-trap beads (Chromotek). Beads were incubated with extracts for 2 h at  $4^{\circ}\text{C}$ , washed and analysed by western blot.

SDS-PAGE was performed using NuPAGE 4–12% Bis-Tris gels (Life Technologies). For western blots, nitrocellulose membranes were developed using horseradish peroxidase (HRP)-coupled antibodies, Supersignal kit (Pierce) and a LAS-3000 imager (Fujifilm).

**Cells and transfections.** hTERT immortalized RPE1 cells (Clontech) were grown in DMEM/HAM F12, MEFs and 293T cells in DMEM, and MDA-MB-231 cells were grown in RPMI. All media were supplemented with 10% FBS (media and serum from PAA Laboratories). All cells and stable clones were found negative for mycoplasma infection by a sensitive PCR assay.

RPE1 cells were electroporated with ECM 630 BTX (Harvard Apparatus). Ten-million cells were resuspended in 200  $\mu\text{l}$  serum-free DMEM/HAM F12 medium containing 7.5 mM HEPES, pH 7.5, mixed with 10–40  $\mu\text{g}$  DNA plasmid in 50  $\mu\text{l}$  210 mM NaCl and electroporated at 1,500  $\mu\text{F}$  and 250 V. To isolate stable Arpin-depleted clones, MDA-MB-231 cells were transfected with shRNA Arpin 3 or shControl using Lipofectamine 2000, and clones selected with  $10\ \mu\text{g}\ \text{ml}^{-1}$  blasticidin (Invivogen) were isolated with cloning rings and expanded. For rescue experiments, cells transfected with shRNA 3, which targets the 3' UTR, were transfected with GFP-Arpin, which lacks UTR sequences. To validate Arpin localization, MEFs were transfected with non-targeting (D-001810-10) or Arpin targeting (J-059240-10; ON-TARGET plus siRNA, Dharmacon) using lipofectamine RNAiMax (Life Technologies), and examined after 2 days.

**Immunofluorescence and live imaging of mammalian cells.** Cells were fixed in 10% TCA, permeabilized with 0.2% Triton X-100, and processed for immunofluorescence. To draw radial line scans, a custom made ImageJ plug-in was developed, edge was determined using 'Isodata' thresholding, then a custom-made VBA macro in Excel was used to align data relative to the edge. Lamellipodial dynamics and random migration were analysed with ImageJ using the plugins 'Kymograph' and 'MtrackJ', respectively. All imaging was done on an Axio Observer microscope (Zeiss) equipped with a Plan-Apochromat 63 $\times$ /1.40 oil immersion objective, an EC Plan-Neofluar 40 $\times$ /1.30 oil immersion objective and a Plan-Apochromat 20 $\times$ /0.80 air objective, a Hamamatsu camera C10600 Orca-R<sup>2</sup> and a Pecon Zeiss incubator XL multi S1 RED LS (Heating Unit XL S, Temp module, CO<sub>2</sub> module, Heating Insert PS and CO<sub>2</sub> cover).

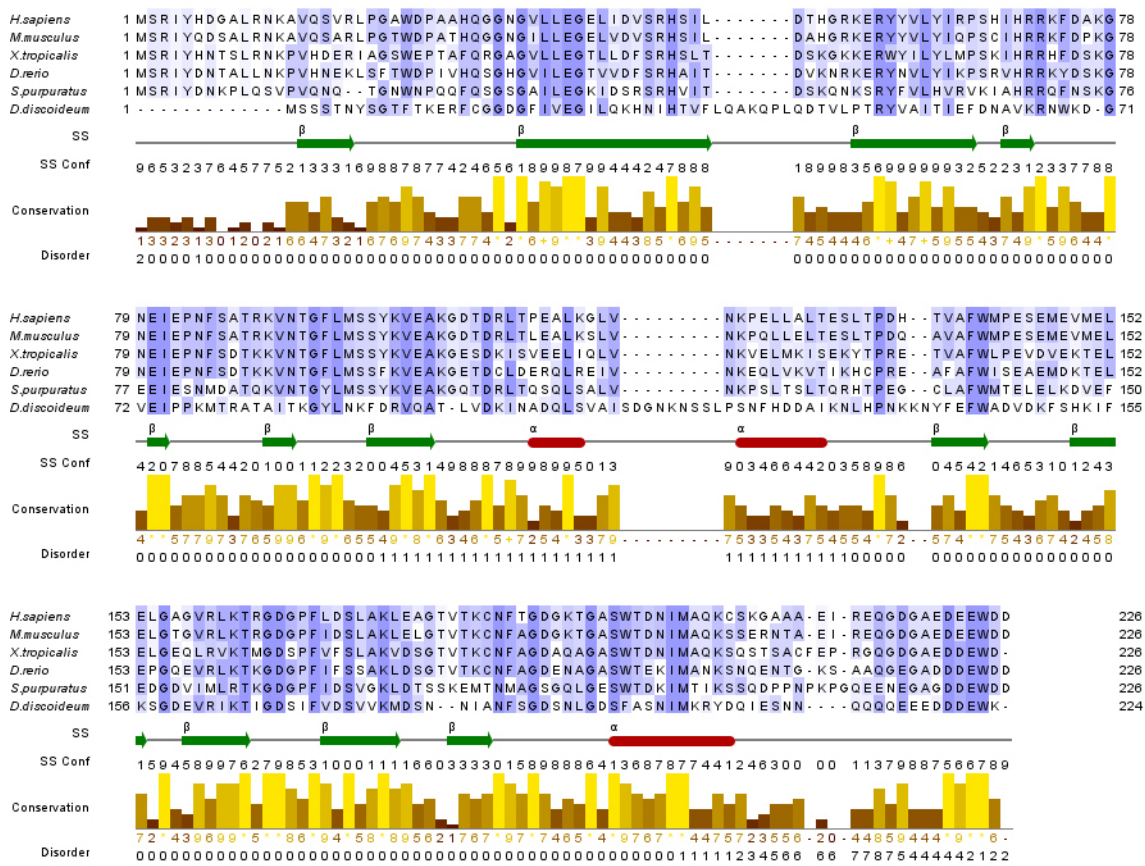
**Fish keratocytes.** Keratocytes were isolated from scales of freshly killed brook trout (*Salvelinus fontinalis*) as previously described<sup>35</sup> and imaged by phase contrast on an inverted Zeiss AxioScope using  $\times 63$  optics, and a halogen lamp as light source. Microinjection was performed with a micromanipulator (Leitz) and a micro-injector Femtojet (Eppendorf) controlling backpressure and injection pulses. Contours were analysed using the CellTrack software (Ohio State University).

**Zebrafish.** Embryos were obtained by natural spawning of *Tg(-1.8gsc:GFP)ml1* fish<sup>36</sup>. In these embryos, prechordal plate cells can be identified by their expression of GFP. *In situ* hybridization was performed following standard protocols<sup>37</sup>. For loss of function experiments, a morpholino directed against *arpin* (GTTGTCAT AAATACGACTCATCTTC, where the underlined anticodon corresponds to the initiating ATG codon), or a standard control morpholino (CCTCTTACCTCAG TTACAATTATA) was injected at the one-cell stage, together with histone2B-mCherry mRNAs or Lifeact-mCherry mRNAs, and GFP-Arpin mRNAs for rescue experiments. To analyse cell trajectories, confocal z-stacks were acquired every minute using a Nikon confocal spinning disk with an Evolve camera (Photometrics). Nuclei were tracked using Imaris (Bitplane). Further analyses were performed using custom routines in Matlab (MathWorks)<sup>38</sup>. All animal studies were done in accordance with the guidelines issued by the French Ministry of Agriculture (Decree no 2013-118) and have been submitted to Paris ethical committee no. 3. **Dictyostelium discoideum.** Cultivation and transformation by electroporation of *D. discoideum* cells was performed as described<sup>39</sup>. To knockout Arpin, a piece of genomic DNA containing the *arpin* coding sequence with its intron was amplified from Ax2 wild-type amoeba, using oligonucleotides DdArpin\_BU 5'-CGCGGATCCGCATGAGTTCAAGTACAAATTATAGT-3' and DdArpin\_SD 5'-CGCGTCCGATTTATTTCCATTCATCATCATCTTC-3'. The cloned PCR fragment was then used as a template to amplify a 5' fragment (using 5'-CGCGGATCCGCATGAGTTCAAGTACAAATTATAGT-3' and 5'-GCGCTGCAGCATCTGA AATTGCAACTGATAGTTG-3') and a 3' fragment (using 5'-GCGAAGCTTTC TTCTTTACCTTCAAATTTTCAT-3' and 5'-CGCGTGCAGCTTGTTATTT GATTCTATTTGATC-3'). These two fragments were cloned as to flank a cassette

carrying Blasticidin resistance in pLPBLP vector<sup>40</sup>. Arpin knockout clones were selected in HL5c-medium supplemented with 10 µg ml<sup>-1</sup> blasticidin S (Invivogen) after electroporation of the resulting vector. Recombination was assessed using diagnostic PCRs that distinguish knockout from wild-type amoeba. GFP-Arpin re-expressing knockout lines were obtained after electroporation of pDGFP-Arpin and selection with 10 µg ml<sup>-1</sup> geneticin (Sigma). Two time series with more than 30 cells each were acquired per amoeba. Two clones isolated after each transformation gave similar results.

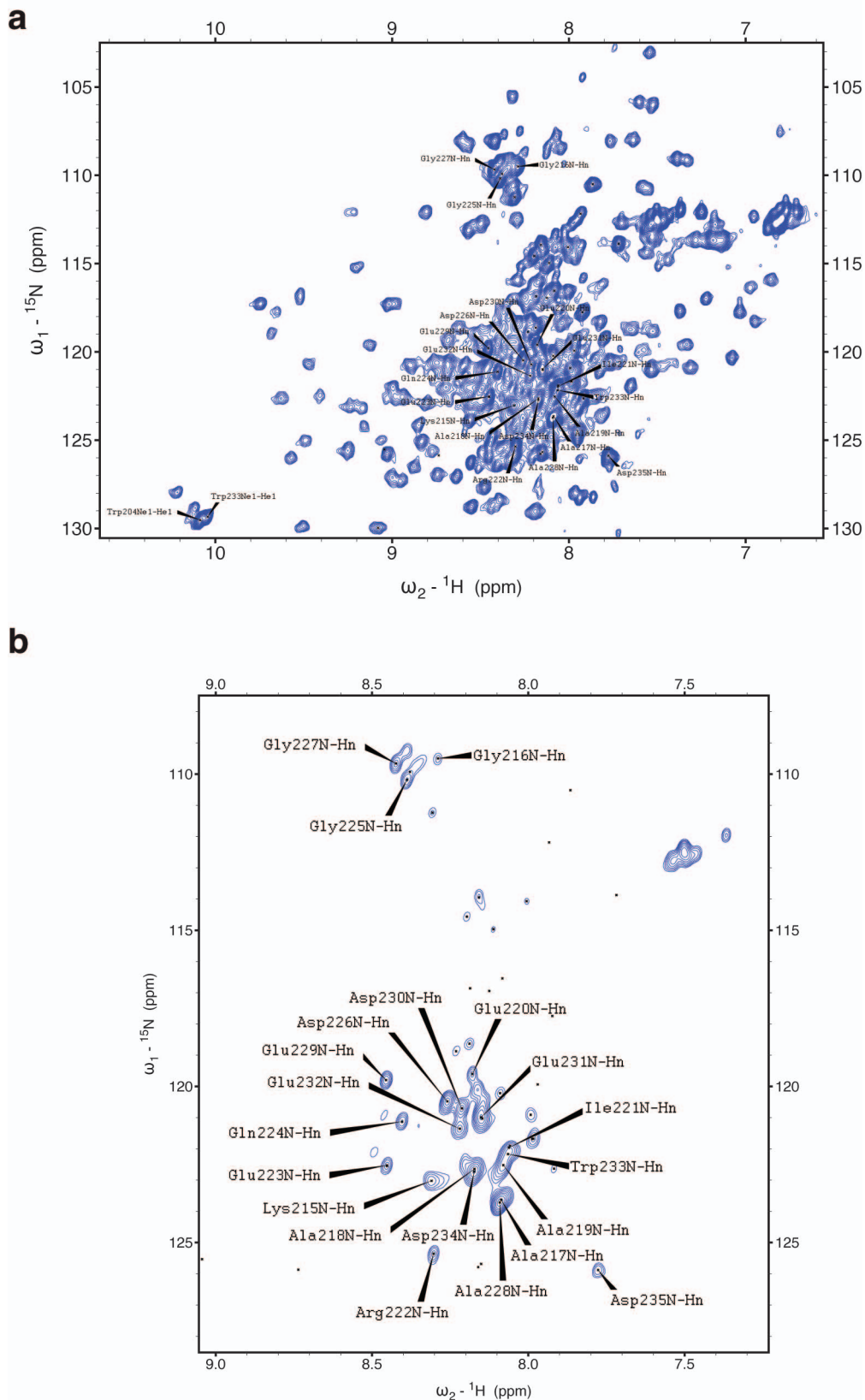
**Statistics.** Statistical analysis of the results was carried out with SigmaStat software (SPSS inc., v2.03). When data satisfied the two criteria of normality and equal variance, parametric tests were used: *t*-test to compare two groups; ANOVA for more than two. Where indicated, a bijective transformation was applied to the data to pass the two criteria of normality and equal variance. When data did not satisfy both criteria even after transformation, non-parametric tests were applied: Mann-Whitney to compare two groups; Kruskal-Wallis for more than two. A representative experiment is plotted and results are expressed as mean s.e.m. with respect to the number of cells (*n*). Differences were considered significant at confidence levels greater than 95% (two-tailed). Three levels of statistical significance are distinguished: \**P* < 0.05; \*\**P* < 0.01; \*\*\**P* < 0.001.

28. Lommel, S. *et al.* Actin pedestal formation by enteropathogenic *Escherichia coli* and intracellular motility of *Shigella flexneri* are abolished in N-WASP-defective cells. *EMBO Rep.* **2**, 850–857 (2001).
29. Millard, T. H., Behrendt, B., Launay, S., Futterer, K. & Machesky, L. M. Identification and characterisation of a novel human isoform of Arp2/3 complex subunit p16-ARC/ARPC5. *Cell Motil. Cytoskeleton* **54**, 81–90 (2003).
30. Dumontier, M., Hocht, P., Mintert, U. & Faix, J. Rac1 GTPases control filopodia formation, cell motility, endocytosis, cytokinesis and development in *Dictyostelium*. *J. Cell Sci.* **113**, 2253–2265 (2000).
31. Derivery, E. *et al.* Free Brick1 is a trimeric precursor in the assembly of a functional wave complex. *PLoS ONE* **3**, e2462 (2008).
32. Michelot, A. *et al.* Actin-filament stochastic dynamics mediated by ADF/cofilin. *Curr. Biol.* **17**, 825–833 (2007).
33. Machesky, L. M. *et al.* Scar, a WASP-related protein, activates nucleation of actin filaments by the Arp2/3 complex. *Proc. Natl Acad. Sci. USA* **96**, 3739–3744 (1999).
34. Marchand, J. B., Kaiser, D. A., Pollard, T. D. & Higgs, H. N. Interaction of WASP/Scar proteins with actin and vertebrate Arp2/3 complex. *Nature Cell Biol.* **3**, 76–82 (2001).
35. Urban, E., Jacob, S., Nemethova, M., Resch, G. P. & Small, J. V. Electron tomography reveals unbranched networks of actin filaments in lamellipodia. *Nature Cell Biol.* **12**, 429–435 (2010).
36. Doitsidou, M. *et al.* Guidance of primordial germ cell migration by the chemokine SDF-1. *Cell* **111**, 647–659 (2002).
37. Hauptmann, G. & Gerster, T. Two-color whole-mount *in situ* hybridization to vertebrate and *Drosophila* embryos. *Trends Genet.* **10**, 266 (1994).
38. Dumortier, J. G., Martin, S., Meyer, D., Rosa, F. M. & David, N. B. Collective mesendoderm migration relies on an intrinsic directionality signal transmitted through cell contacts. *Proc. Natl Acad. Sci. USA* **109**, 16945–16950 (2012).
39. Schirenbeck, A., Bretschneider, T., Arasada, R., Schleicher, M. & Faix, J. The Diaphanous-related formin dDia2 is required for the formation and maintenance of filopodia. *Nature Cell Biol.* **7**, 619–625 (2005).
40. Faix, J., Kreppel, L., Shaulsky, G., Schleicher, M. & Kimmel, A. R. A rapid and efficient method to generate multiple gene disruptions in *Dictyostelium discoideum* using a single selectable marker and the *Cre-loxP* system. *Nucleic Acids Res.* **32**, e143 (2004).
41. Edgar, R. C. MUSCLE: multiple sequence alignment with high accuracy and high throughput. *Nucleic Acids Res.* **32**, 1792–1797 (2004).
42. Clamp, M., Cuff, J., Searle, S. M. & Barton, G. J. The Jalview Java alignment editor. *Bioinformatics* **20**, 426–427 (2004).
43. McGuffin, L. J., Bryson, K. & Jones, D. T. The PSIPRED protein structure prediction server. *Bioinformatics* **16**, 404–405 (2000).
44. Ward, J. J., McGuffin, L. J., Bryson, K., Buxton, B. F. & Jones, D. T. The DISOPRED server for the prediction of protein disorder. *Bioinformatics* **20**, 2138–2139 (2004).
45. Blanchoin, L. *et al.* Direct observation of dendritic actin filament networks nucleated by Arp2/3 complex and WASP/Scar proteins. *Nature* **404**, 1007–1011 (2000).
46. Montero, J. A., Kilian, B., Chan, J., Bayliss, P. E. & Heisenberg, C. P. Phosphoinositide 3-kinase is required for process outgrowth and cell polarization of gastrulating mesendodermal cells. *Curr. Biol.* **13**, 1279–1289 (2003).



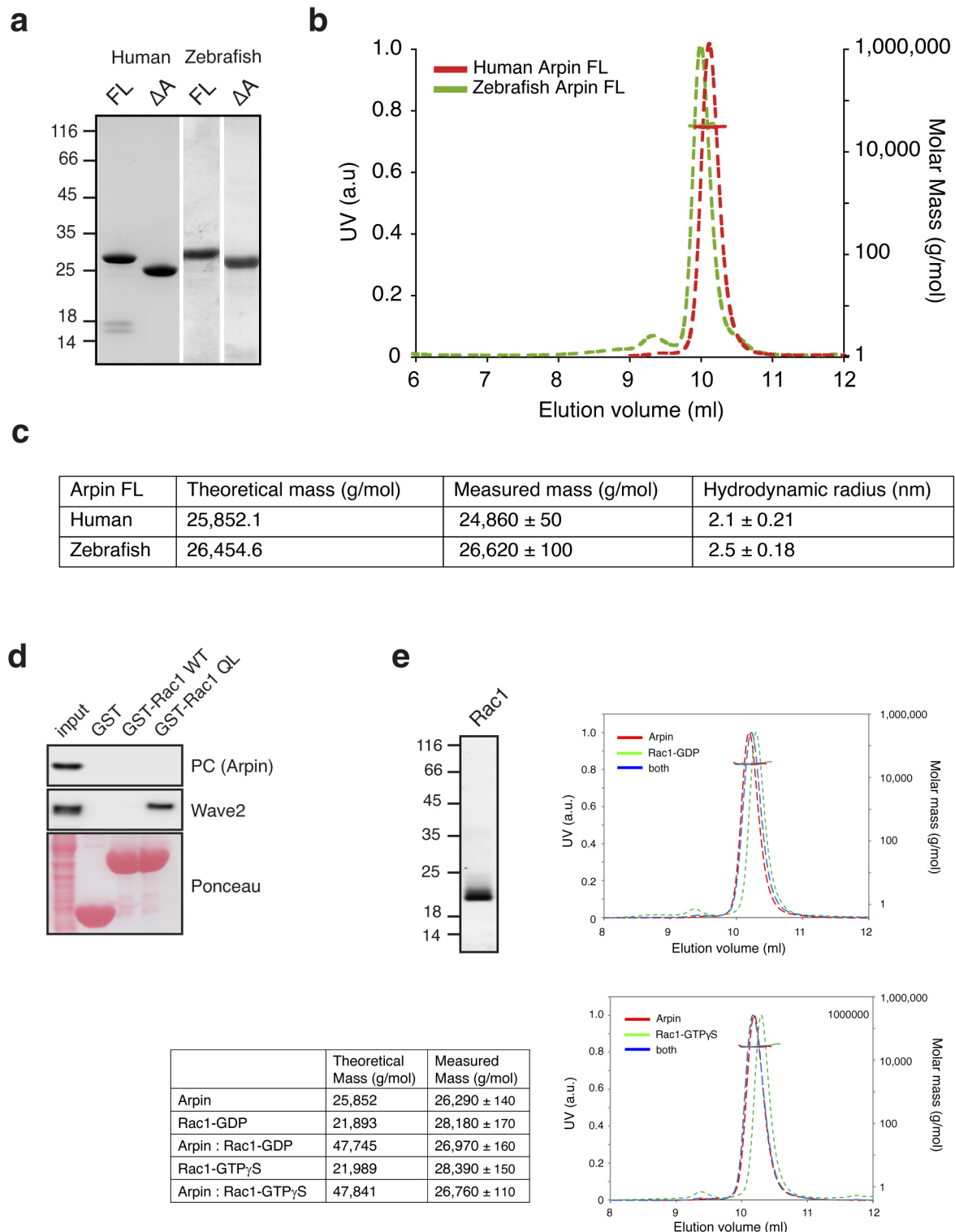
**Extended Data Figure 1 | Prediction of secondary structure elements and disordered regions of Arpin.** A multiple alignment of the Arpin orthologues was performed with MUSCLE<sup>41</sup> and displayed with Jalview<sup>42</sup>. Two methods relying on multiple alignments of Arpin orthologues were used to predict secondary structures and disordered regions, Pspipred<sup>43</sup> and Disopred<sup>44</sup>, respectively. The predicted secondary structure (SS) elements are indicated by green arrows for  $\beta$ -strands, red cylinders for  $\alpha$ -helices, and a black line for coils;

the associated confidence (conf) score is displayed below, ranging from 0 to 9 for poor and high confidence, respectively. Amino acid conservation is indicated by a 0 to 10 score, and highlighted by brown to yellow histogram bars. The confidence in predicting disorder is also scored from 0 to 10, by multiplying tenfold the Disopred probability. Arpin is predicted to be a structured protein with the notable exception of the 20 C-terminal residues, which are predicted to be disordered with high confidence.



**Extended Data Figure 2** | NMR analysis of  ${}^{15}\text{N}$ -labelled human Arpin. Both views represent  ${}^1\text{H}$ - ${}^{15}\text{N}$  heteronuclear single quantum coherence (HSQC) spectra. Each peak corresponds to the  ${}^1\text{H}$ - ${}^{15}\text{N}$  backbone amide bond of a specific residue. The position of a  ${}^1\text{H}$ - ${}^{15}\text{N}$  peak in the spectrum depends on the chemical environment of the corresponding residue. **a**, Such a scattered distribution of peaks is characteristic of a folded protein. The last 20 residues were assigned to individual peaks and are displayed on the spectrum. These

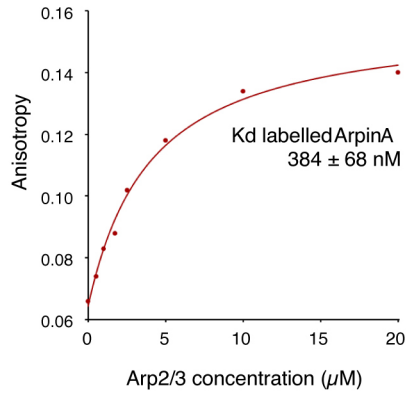
residues are clustered in the centre of the spectrum. **b**, Same HSQC spectrum displayed with a higher threshold to display only high peaks. The height of a peak depends on the mobility of the residue on a picosecond to millisecond timescale. This spectrum experimentally demonstrates that the 20 C-terminal residues are highly mobile. This result confirms that, as predicted, the Arp2/3-binding site of Arpin is exposed as a poorly structured tail of the protein.



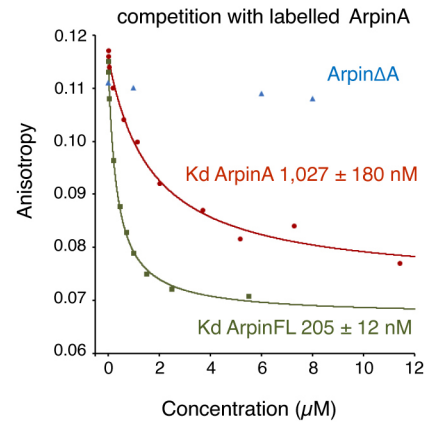
**Extended Data Figure 3 | Characterization of recombinant Arpin.** **a**, Full-length Arpin or Arpin $\Delta$ A from human or zebrafish cDNA was expressed in *E. coli* and purified. Purity was assessed by SDS-PAGE and coomassie staining. These proteins were used for *in vitro* actin polymerization assays and for fish keratocyte injection, respectively. **b**, Analysis of the molar mass of full-length Arpins by size-exclusion chromatography coupled to multiangle light scattering (SEC-MALS). The ultraviolet measurement (left axis, dashed line) and the molar mass (right axis, horizontal solid line) were plotted as a function of column elution volume. **c**, SEC-MALS measures of masses indicate that both proteins are monomeric in solution. **d**, GST pull-down using a lysate of 293 cells overexpressing PC-tagged Arpin and purified GST-Rac1 wild type,

GST-Rac1(Gln61Leu) or GST alone as a negative control. Arpin did not associate with either type of Rac. By contrast, the endogenous WAVE complex bound to Rac(Gln61Leu), but not Rac wild type, as expected from a Rac effector. **e**, Untagged Rac1 was purified from *E. coli* and then loaded with either GDP or GTP $\gamma$ S. Human Arpin (60  $\mu$ M), Rac1 (120  $\mu$ M) and mixture of these two proteins were analysed by SEC-MALS as above. SEC was run in 20 mM HEPES, 100 mM NaCl, pH 7.4. The height of ultraviolet peaks was normalized to 1 to be displayed on the same figure. A single peak was detected in all cases. The measured masses indicate that no complex is formed between Arpin and Rac and that the single peak observed in the mixture corresponds to cofractionation of the two proteins of similar mass by SEC.

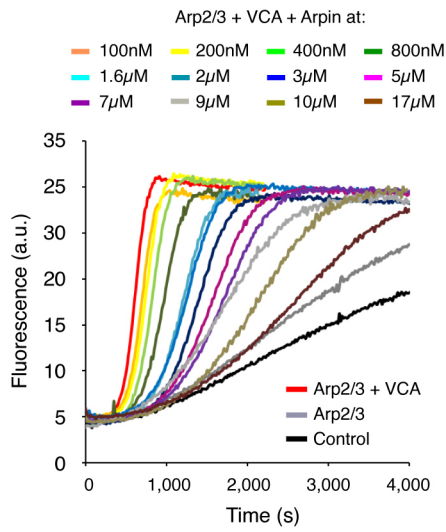
**a**



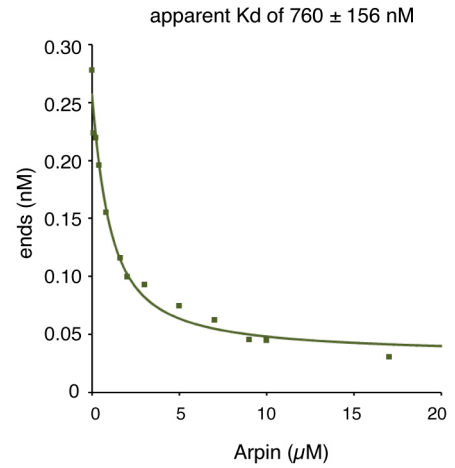
**b**



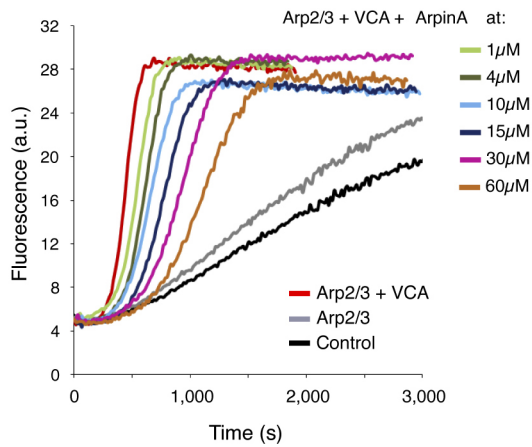
**c**



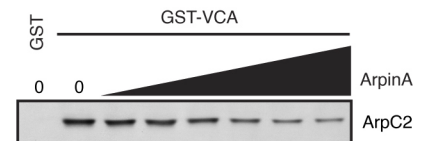
**d**



**e**



**f**



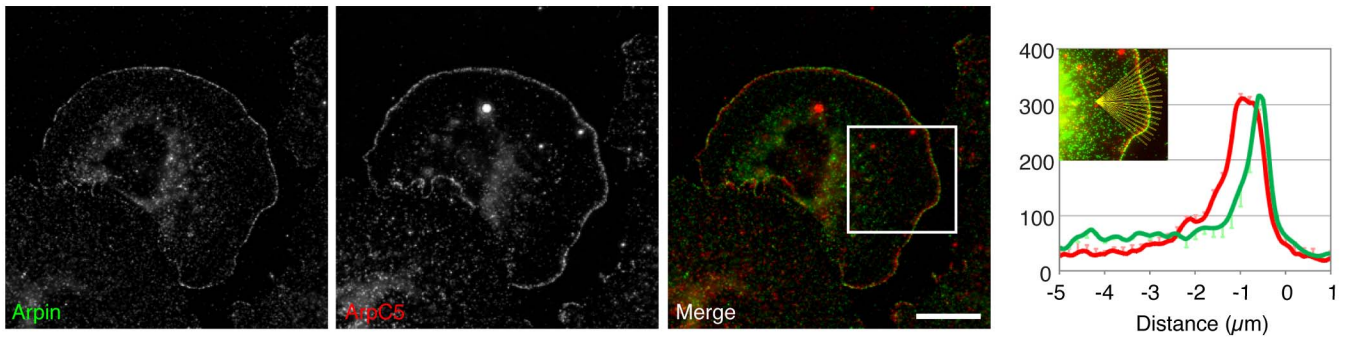
**Extended Data Figure 4 | Arpin directly binds to the Arp2/3 complex.**

**a**, Fluorescence anisotropy measurements of labelled ArpinA peptide binding at equilibrium to the purified Arp2/3 complex at the indicated concentrations.

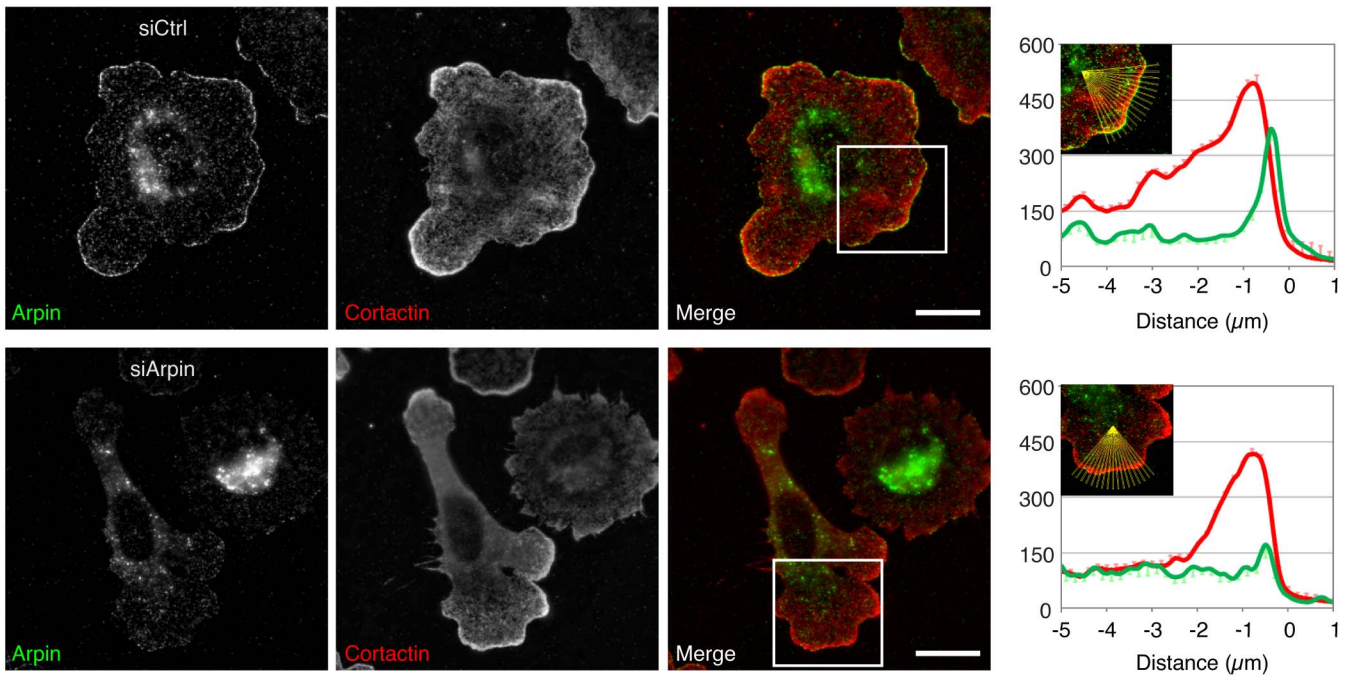
**b**, Labelled ArpinA peptide bound to the Arp2/3 complex was then titrated with purified Arpin full-length, Arpin $\Delta$ A or unlabelled ArpinA peptide as indicated. Full-length Arpin displaces the labelled ArpinA peptide more efficiently than the A peptide. Arpin $\Delta$ A is unable to displace the ArpinA peptide. Curves that best fit the values yield the indicated equilibrium constants. **c**, Arpin inhibits Arp2/3 activation in the pyrene-actin assay. Part of this experiment is displayed in Fig. 1c, more curves are plotted here. **d**, From curves in c, the number of actin

barbed ends is calculated from the slope at half-polymerization using the relationship described previously<sup>45</sup>. Best fit of the values indicate an apparent  $K_d$  value of  $760 \pm 156$  nM for the Arp2/3 complex in a mixture including actin and the VCA. **e**, ArpinA inhibits Arp2/3 activation in a dose dependent manner in the pyrene-actin assay. Conditions: 2  $\mu$ M actin (10% pyrene-labelled), 500 nM VCA, 20 nM Arp2/3 and ArpinA at the indicated concentrations. **f**, ArpinA competes with the NPF for Arp2/3 binding. Arp2/3 is displaced from its interaction with 5  $\mu$ M GST N-WASP VCA immobilized on glutathione beads by the Arpin acidic peptide (304  $\mu$ M and serial twofold dilutions).

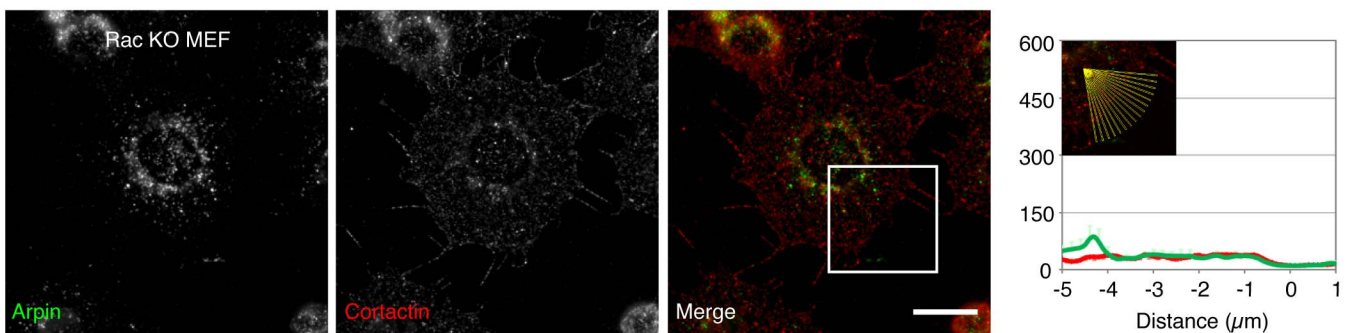
a



b

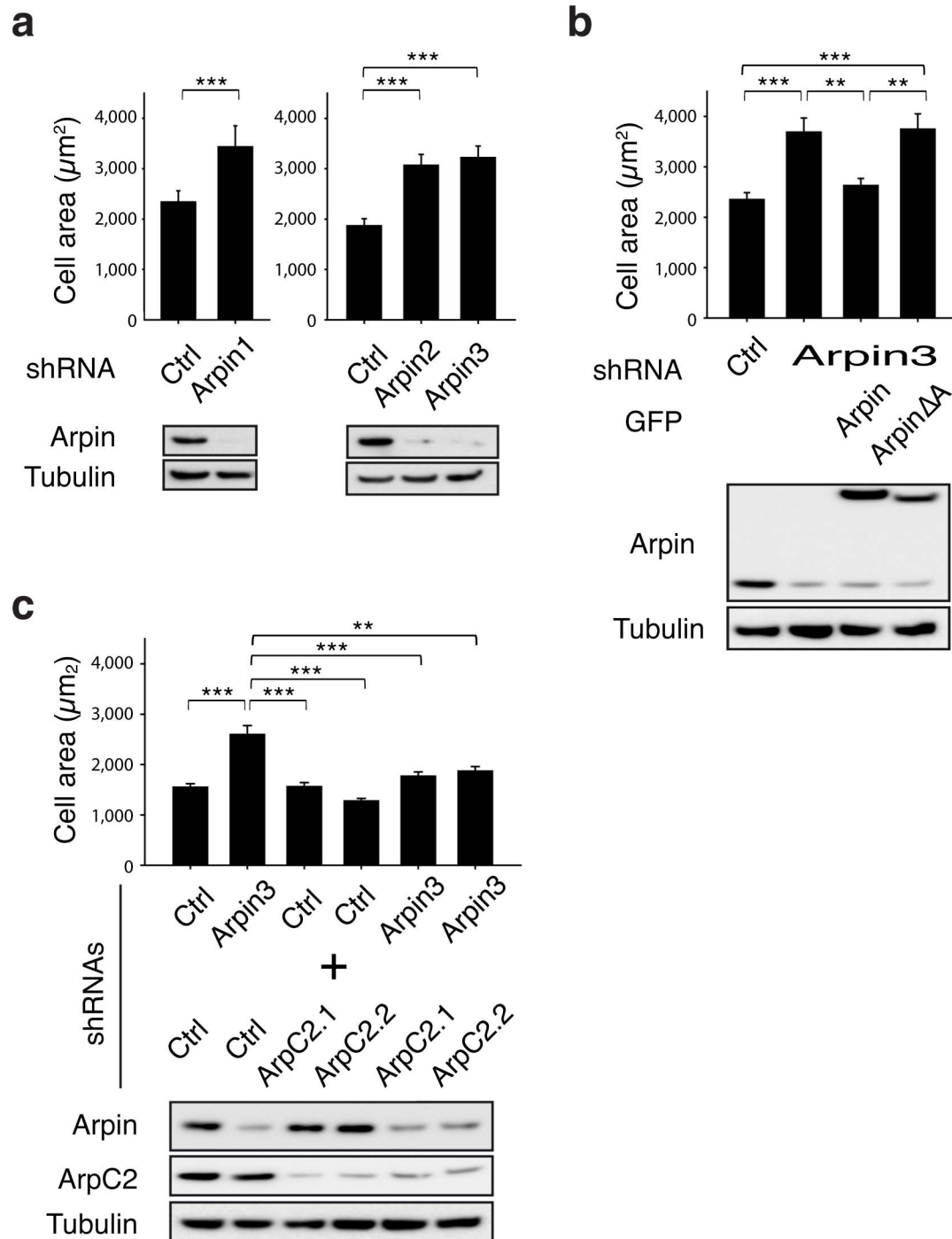


c



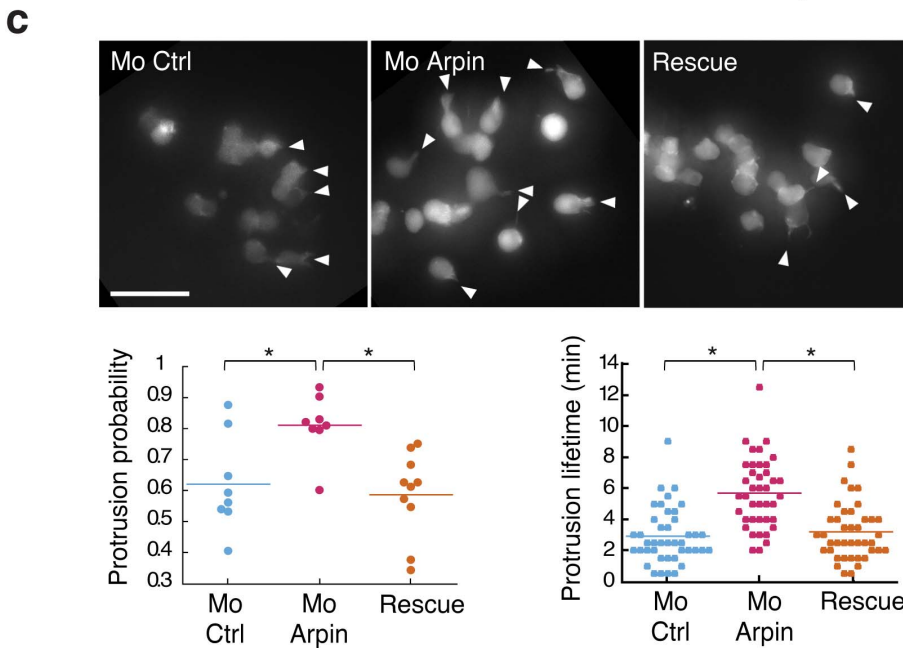
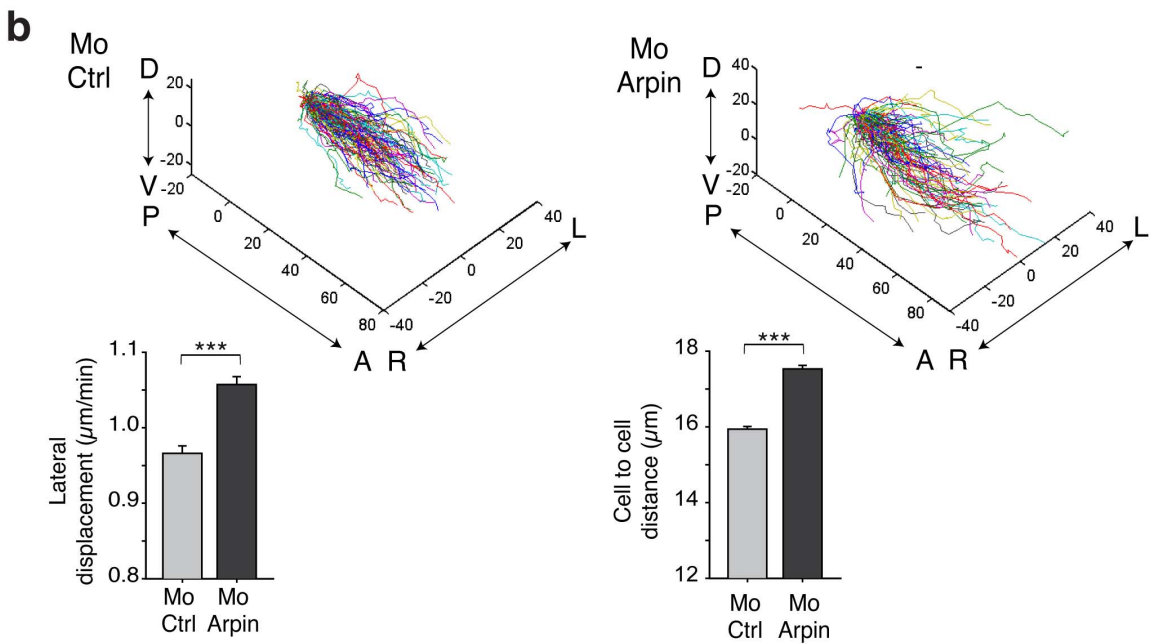
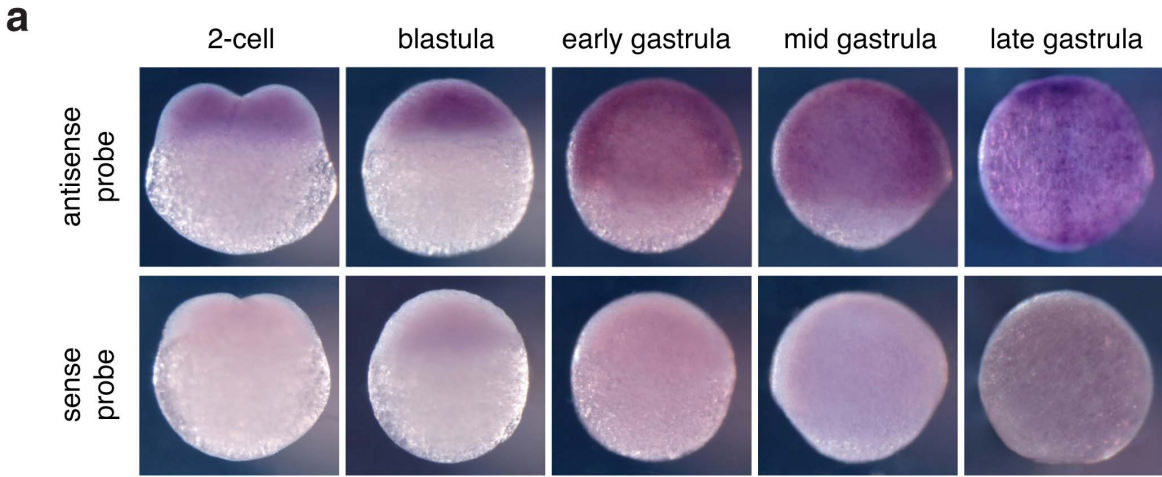
**Extended Data Figure 5 | Specific localization of Arpin at the lamellipodium tip.** **a**, Arpin overlaps with the Arp2/3 complex at the lamellipodium tip. **b**, Arpin overlaps with cortactin at the lamellipodium tip. Arpin staining is lost after short interfering RNA (siRNA)-mediated depletion. Intensity profiles along multiple line scans encompassing the cell periphery were registered to the outer edge of the staining of a lamellipodial marker. This marker was Arpin in **a** and cortactin in **b**. The multiple line scans were then averaged and displayed as an intensity plot, where the  $y$  axis represents fluorescent intensity, arbitrary units (mean  $\pm$  s.e.m.,  $n = 17$ , 16 and 17, respectively). Scale bar, 20  $\mu\text{m}$ . Arp2/3 localization extends rearwards relative to Arpin localization. This result is because the Arp2/3 complex becomes a branched junction when activated by the WAVE complex at the lamellipodium

tip. The branched junction undergoes retrograde flow like actin itself due to actin filament elongation<sup>9,12</sup>. Cortactin recognizes Arp2/3 at the branch junction and is thought to stabilize branched actin networks<sup>13</sup>. As a marker of the branched junction, cortactin stains the width of lamellipodia<sup>14</sup> like the Arp2/3 complex. **c**, Rac1 knockout MEFs that lack lamellipodia<sup>14</sup> are completely devoid of Arpin staining at the cell periphery, in line with the complete absence of lamellipodia indicated here by the absence of cortactin staining. Arpin is normally expressed in the Rac1 knockout MEFs (see Fig. 2c). Intensity profiles along multiple line scans encompassing the cell periphery were averaged after manual drawing of the cell edge (mean  $\pm$  s.e.m.,  $n = 16$ ). Scale bar, 20  $\mu\text{m}$ .



**Extended Data Figure 6 | Arpin regulates cell spreading through its interaction with the Arp2/3 complex.** Arpin was depleted from human RPE1 cells after transient transfection of shRNA plasmids and blasticidin-mediated selection of transfected cells. After 5 days, cells were either analysed by western blot or used for the spreading assay. Cells were serum-starved for 90 min in suspension in polyHEMA-coated dishes and then allowed to spread on collagen-I-coated coverslips for 2 h. Phalloidin staining was used to calculate cell surface area of individual cells using ImageJ. Mean  $\pm$  s.e.m.; \*\* $P < 0.01$ , \*\*\* $P < 0.001$ ; *t*-test or ANOVA when more than two conditions. **a**, Arpin

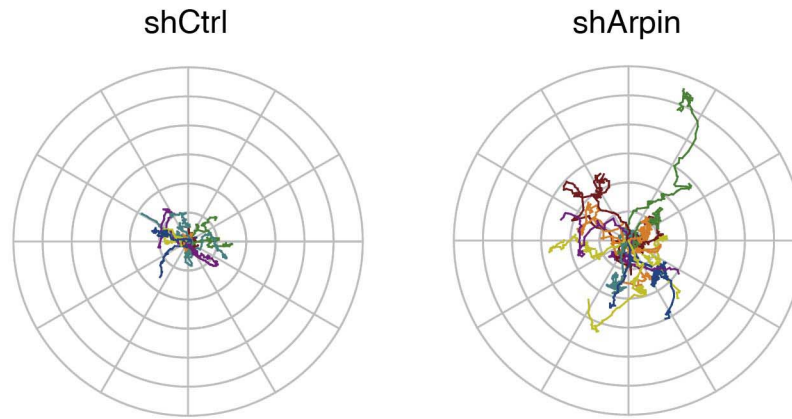
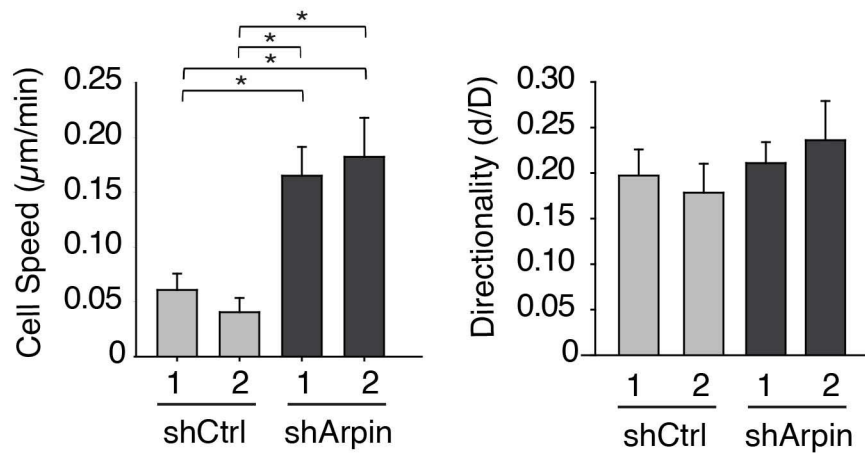
depletion increases cell spreading ( $n = 57$  and  $52$ , respectively). The same effect is obtained with three shRNAs targeting Arpin ( $n = 51$ ,  $48$  and  $59$ , respectively). **b**, This effect is rescued by GFP–Arpin expression in knockdown cells, but not by GFP–ArpinΔA expression ( $n = 63$ ,  $56$ ,  $63$  and  $52$ , respectively). **c**, Combined depletion of Arpin and the Arp2/3 complex reverses the phenotype of Arpin depletion. The effect is seen with two shRNAs targeting ArpC2 ( $n = 56$ ,  $60$ ,  $69$ ,  $68$ ,  $63$  and  $66$ , respectively). The last two experiments indicate that Arpin exerts its effect on cell spreading through its ability to regulate the Arp2/3 complex.



**Extended Data Figure 7 | Arpin regulates protrusion frequency of prechordal plate cells and their collective migration in zebrafish embryos.**

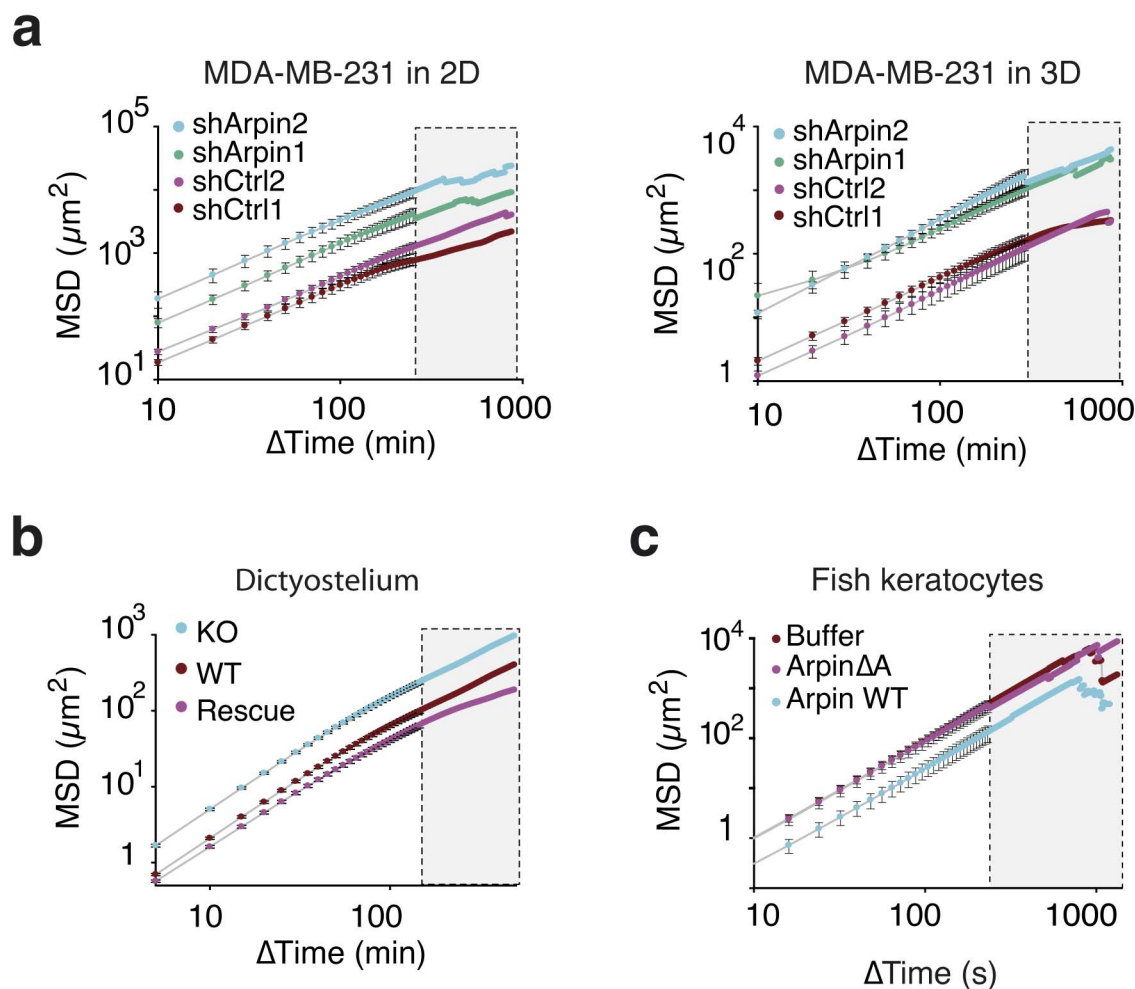
**a**, *In situ* hybridization of *arpin* probe in zebrafish embryos at different stages. *arpin* mRNAs are maternally deposited. During gastrulation, *arpin* is expressed in hypoblast, which includes the prechordal plate. **b**, Three-dimensional trajectories of prechordal plate cells in embryos injected with control or *arpin* morpholino. During fish gastrulation, prechordal plate cells migrate collectively in a straight direction from the margin of the embryo towards the animal pole<sup>38,46</sup>. Loss of *arpin* function induces dispersion as evidenced by increased lateral cell displacement ( $n = 1,516$  and  $1,546$ ) and a higher distance between cells ( $n = 194$  and  $235$ ). Lateral displacement is the cell movement perpendicular to main direction of the migration. Distance between cells refers to the average distance of the nucleus of a given cell to the nuclei of its five closest neighbours. Mean  $\pm$  s.e.m.; \*\*\* $P < 0.001$ , *t*-test. **c**, At the onset of

gastrulation prechordal plate cells derived from morpholino injected embryos were transplanted into the prechordal plate of an untreated host embryo at the same stage in order to allow imaging of cell autonomous effects on protrusion formation. Donor embryos are injected with control or *arpin* morpholinos and mRNAs encoding Lifeact-mCherry as well as GFP-Arpin for the rescue. Time-lapse imaging of injected cells is performed by epifluorescence to reveal Lifeact, a marker of filamentous actin, which stains actin-based protrusions. For each cell, presence of a protrusion was assessed at each frame to deduce probability of protrusion presence and protrusion lifetimes. *arpin* loss of function increases the probability of presence of protrusions ( $n = 8, 8$  and  $10$ , respectively; \* $P < 0.05$ , ANOVA) and their duration (in this case,  $n$  corresponds to the number of protrusions ( $n = 42, 41$  and  $40$ , respectively; \* $P < 0.05$ , Kruskal-Wallis). Protrusions are indicated by arrowheads. Scale bar,  $50 \mu\text{m}$ .

**a****b**

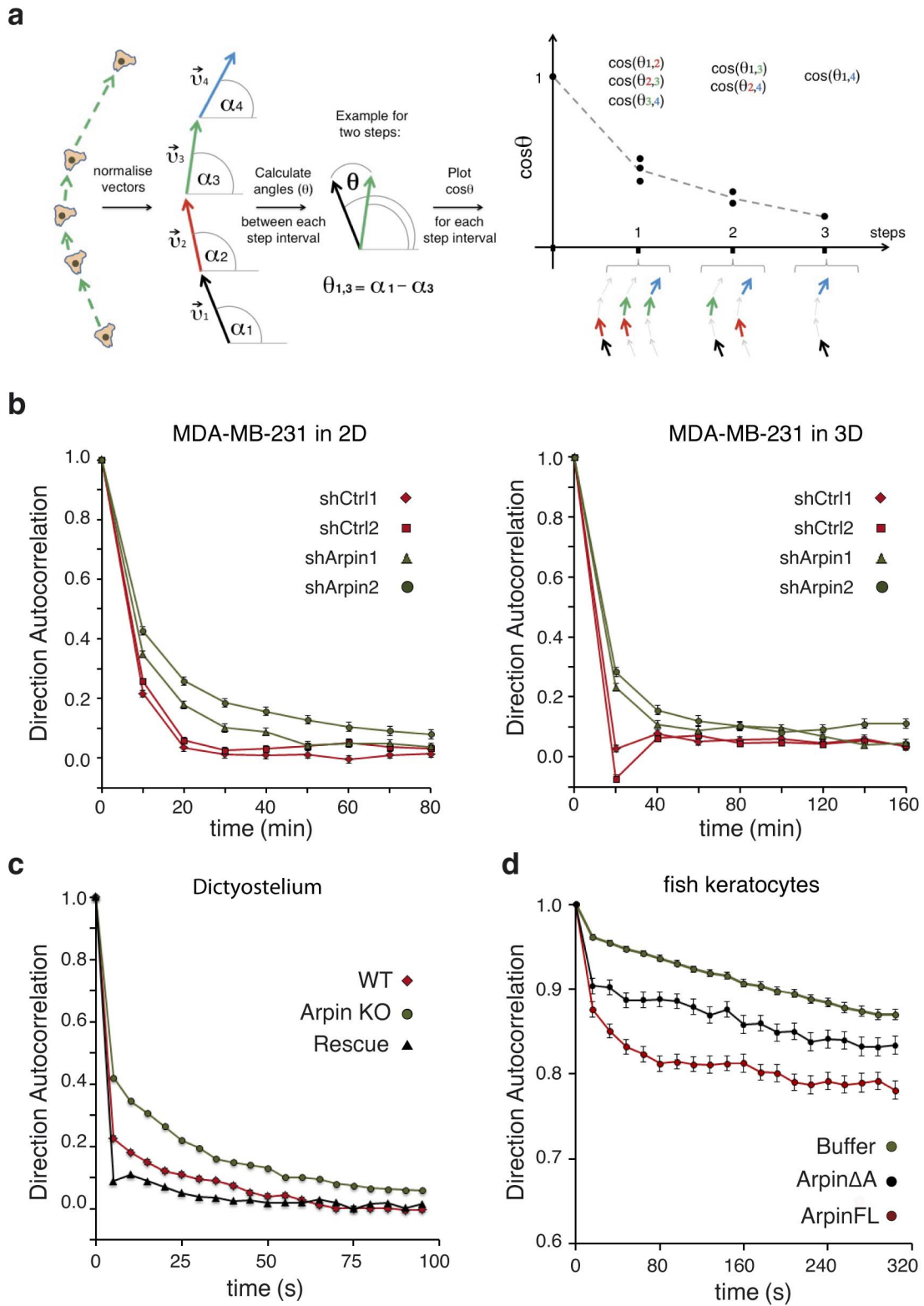
**Extended Data Figure 8 | Arpin depletion increases cell migration in three dimensions.** Stable MDA-MB-231 clones depleted of Arpin or not were embedded in a collagen gel. **a**, Single-cell trajectories illustrate that control cells hardly move in this dense environment (see Supplementary Video 4), unlike Arpin-depleted cells, which explore a significant territory, albeit at lower pace than in two dimensions, as evidenced by mean square displacement (Extended

Data Fig. 9). **b**, Cell speed is significantly increased in the Arpin-depleted clones. Mean  $\pm$  s.e.m.;  $n = 27, 25, 26$  and  $17$ , respectively,  $*P < 0.05$ , Kruskal–Wallis, two experiments. Directional persistence, calculated by  $d/D$ , is not significantly different in the clones depleted of Arpin or not. Direction autocorrelation (Extended Data Fig. 10), however, shows an increased directionality in the Arpin-depleted cells at the earliest time points.



**Extended Data Figure 9 | Analysis of mean square displacement of the different migration experiments.** The mean square displacement gives a measure of the area explored by cells for any given time interval. By setting a positional vector on the cellular trajectory at time  $t$ , the MSD is defined as:  $MSD(\Delta t) = \langle [x(t+t_0) - x(t_0)]^2 + [y(t+t_0) - y(t_0)]^2 \rangle_{t,N}$ , in which brackets  $\langle \rangle$  indicate averages over all starting times  $t_0$  and all cells  $N$ . For each time interval  $\Delta t$ , mean and s.e.m. are plotted. Error bars corresponding to s.e.m. are plotted, even if too small to be visible. The grey area excludes the noisy part of curves corresponding to large time intervals where less data points are available. **a**, MDA-MB-231 depleted or not of Arpin in a two- or three-dimensional

environment. Arpin-depleted MDA-MB-231 cells explore a larger territory than the controls in time intervals examined (for two dimensions,  $n$  as indicated in Fig. 3a;  $P < 0.001$ , two-way ANOVA with time and conditions; for three dimensions,  $n$  as indicated in Extended Data Fig. 8;  $P < 0.001$ , two-way ANOVA with time and conditions). **b**, *Dictyostelium discoideum* knockout amoebae explore a larger territory than controls and rescued amoebae ( $n$  as indicated in Fig. 3b,  $P < 0.001$ , two-way ANOVA with time and conditions). **c**, Arpin-injected fish keratocytes explore a smaller territory than the controls ( $n$  as indicated in Fig. 4b;  $P < 0.001$ , two-way ANOVA with time and conditions).



**Extended Data Figure 10 | Analysis of direction autocorrelation of the different migration experiments.** **a**, Principle of the analysis. A hypothetical cell trajectory is depicted. Each step is represented by a vector of normalized length.  $\theta$  is the angle between compared vectors. The plot illustrates the  $\cos\theta$  values for the putative trajectory of four steps (colour-coded). Averaging these  $\cos\theta$  values yields the direction autocorrelation (DA) function of time that measures the extent to which these vectors are aligned over different time intervals. The DA function is defined as:  $DA(t) = \langle v(t_0) \cdot v(t_0 + t) \rangle_{t_0, N} = \langle \cos\theta(t_0, t_0 + t) \rangle_{t_0, N}$ , in which  $v(t_0)$  is the vector at the starting time  $t_0$ , and  $v(t_0 + t)$  the vector at  $t_0 + t$ . Brackets indicate that all calculated cosines are averaged for all possible starting times ( $t_0$ ) over all cells ( $N$ ). For each time interval  $t$ , vectors from all cell trajectories were

used to compute average and sem. Error bars corresponding to s.e.m. are plotted, even if too small to be visible. **b**, Arpin-depleted MDA-MB-231 clones turn less than control cells (for two dimensions,  $n$  as indicated in Fig. 3a;  $P < 0.05$  between 10 and 40 min, Kruskal–Wallis; for three dimensions,  $n$  as indicated in Extended Data Fig. 8;  $P < 0.05$  at time 10 min, Kruskal–Wallis). **c**, Arpin knockout amoebae turn less than wild-type amoebae, and GFP–Arpin overexpressing knockout amoebae (rescue) turn more than wild type ( $n$  as indicated in Fig. 3b;  $P < 0.05$  between 5 and 85 s, Kruskal–Wallis). **e**, Arpin-injected fish keratocytes turn more than buffer-injected cells, and Arpin $\Delta A$ -injected keratocytes turn more than buffer-injected but less than full-length-Arpin-injected keratocytes ( $n$  as indicated in Fig. 4b;  $P < 0.05$  between 16 and 272 s, Kruskal–Wallis).